

Accepted Manuscript

Design, synthesis, and identification of a novel naphthalamide-isoselenocyanate compound NISC-6 as a dual Topoisomerase-II α and Akt pathway inhibitor, and evaluation of its anti-melanoma activity

Deepkamal N. Karelia, Ugir Hossain Sk, Parvesh Singh, A.S. Prakasha Gowda, Manoj K. Pandey, Srinivasa R. Ramiseti, Shantu Amin, Arun K. Sharma

PII: S0223-5234(17)30318-5

DOI: [10.1016/j.ejmech.2017.04.052](https://doi.org/10.1016/j.ejmech.2017.04.052)

Reference: EJMECH 9403

To appear in: *European Journal of Medicinal Chemistry*

Received Date: 9 December 2016

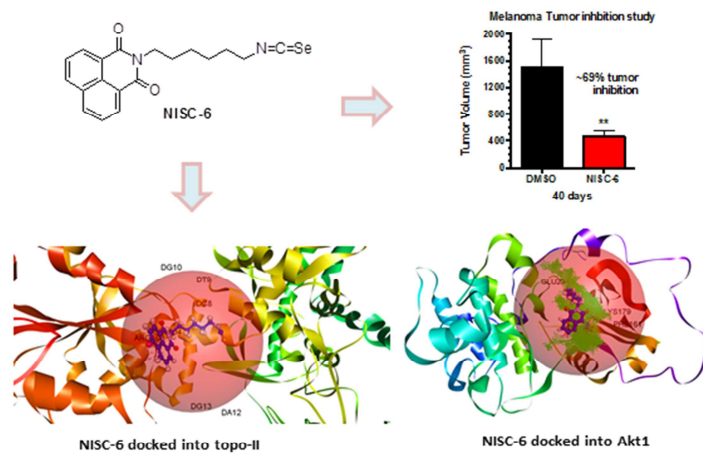
Revised Date: 11 April 2017

Accepted Date: 20 April 2017

Please cite this article as: D.N. Karelia, U.H. Sk, P. Singh, A.S.P. Gowda, M.K. Pandey, S.R. Ramiseti, S. Amin, A.K. Sharma, Design, synthesis, and identification of a novel naphthalamide-isoselenocyanate compound NISC-6 as a dual Topoisomerase-II α and Akt pathway inhibitor, and evaluation of its anti-melanoma activity, *European Journal of Medicinal Chemistry* (2017), doi: 10.1016/j.ejmech.2017.04.052.

This is a PDF file of an unedited manuscript that has been accepted for publication. As a service to our customers we are providing this early version of the manuscript. The manuscript will undergo copyediting, typesetting, and review of the resulting proof before it is published in its final form. Please note that during the production process errors may be discovered which could affect the content, and all legal disclaimers that apply to the journal pertain.





Design, synthesis, and identification of a novel naphthalamide-isoselenocyanate compound NISC-6 as a dual Topoisomerase-II α and Akt pathway inhibitor, and evaluation of its anti-melanoma activity

Deepkamal N. Karelia¹, Ugir Hossain Sk², Parvesh Singh³, A. S. Prakasha Gowda⁴, Manoj K. Pandey^{1,5}, Srinivasa R. Ramiseti¹, Shantu Amin¹, and Arun K. Sharma^{1,*}

¹Department of Pharmacology; Penn State Cancer Institute, CH72; ⁴Department of Biochemistry and Molecular Biology, Penn State College of Medicine, 500 University Drive, Hershey, PA 17033, USA.

²CSIR-Institute of Himalayan Bioresource Technology, Palampur, HP, India

³School of Chemistry and Physics, University of Kwa-Zulu Natal (UKZN), Westville campus, Durban 4000, South Africa

⁵Department of Biomedical Sciences, Cooper Medical School of Rowan University, 401 S Broadway, Camden, NJ 08103 (*current address*)

* Author to whom correspondence should be addressed

Arun K. Sharma, Ph.D.
Department of Pharmacology
Penn State College of Medicine
Penn State Cancer Institute, CH72
Penn State Milton S. Hershey Medical Center
500 University Drive
Hershey, PA 17033

Phone: 717-531-4563
Fax: 717-531-0244
E-mail: aks14@psu.edu

Abstract

Synthesis and anti-melanoma activity of novel naphthalimide isoselenocyanate (NISC) and naphthalimide selenourea (NSU) analogs are described. The novel agents were screened for growth inhibition of different human melanoma cell lines including those having BRAF^{V600E} mutation (UACC903, 1205Lu, and A375M) and BRAF^{WT} (CHL-1). In general, the NISC analogs (**4a-d**) were more effective in inhibiting the cell viability than the NSU analogs (**7a-b**). Overall, NISC-6 (**4d**), having a six-carbon alkyl chain, was identified as the most cytotoxic compound in both BRAF^{V600E} mutated and BRAF^{WT} cells. NISC-6 docked strongly into the binding sites of Akt1 and human topoisomerase II α (Topo-II α), and the docking results were supported by experimental findings showing NISC-6 to inhibit of both Akt pathway and Topo-II α activity in a dose dependent manner. Furthermore, NISC-6 effectively induced apoptosis in human melanoma cells, inhibited tumor growth by ~69% in a melanoma mouse xenograft model, and showed excellent compliance with the Lipinski' rule of five, suggesting both its efficacy and drug-like behavior under physiological conditions.

Keywords: Naphthalimide, isoselenocyanate, selenourea, melanoma, apoptosis, anti-tumor

1. Introduction

Melanoma accounts for less than 5% of skin cancer cases, but causes more than 75% of skin cancer deaths. The vast majority of melanomas can be attributed to exposure to ultraviolet (UV) radiation from the sun [1]. The incidence and mortality rate for melanoma continue to rise [2]; an estimated 87,110 new cases of invasive melanoma will be diagnosed and an estimated 9,730 people will die of melanoma in the U.S. in 2017 [3]. However, no effective treatment currently exists for patients suffering from the metastatic stage of this disease [4], which has poor prognosis and is refractory to most conventional chemotherapies. Currently, the limited treatment options for melanoma patients include dacarbazine and temozolomide, but both have a disappointing response rate. The BRAF^{V600E} inhibitor PLX4032 (vemurafenib) approved recently [5, 6], has shown great therapeutic promise but suffers from onset of resistance in about 7 months [7-11] leading to unsatisfactory outcomes. The combination therapies being tested in clinical trials have also shown limited success. Multiple antibodies against programmed cell death-1 (PD-1) and its ligand (PDL-1) are in development and have shown promise in melanoma and other malignancies. Two of these, Opdivo (BMY) and Keytruda (Merck), were recently approved by FDA for metastatic melanoma in 2014. However, despite clinical benefits, the checkpoint inhibition is associated with a unique spectrum of side effects termed immune-related adverse events (irAEs) that include dermatologic, gastrointestinal, hepatic, endocrine, and other inflammatory events [12].

To address this unmet need, our laboratory has been involved extensively, over the last eight years, in developing novel agents to treat melanoma [13-16]. We earlier developed isoselenocyanate (ISC) compounds based on naturally occurring isothiocyanates (ITCs) that inhibited melanoma tumor growth by targeting the Akt signaling pathway [13, 14]. Naturally

occurring and synthetic phenylalkyl ITCs [17-19] are well established anti-cancer agents against a variety of organ sites [20, 21]. Our structural activity relationship (SAR) studies directed towards the isosteric replacement of sulfur (S) in ITCs by selenium (Se) and varying the alkyl chain length connecting the phenyl ring and the ISC functionality, led to the identification of phenylbutyl isoselenocyanate (ISC-4) as the most promising agent in this series of compounds [13]. ISC-4 was found to be an effective anti-cancer agent [13, 16, 22, 23], being particularly effective against melanoma [13, 14, 16]. It inhibited Akt signaling pathway and significantly retarded melanoma tumor growth without any systemic toxicity [13, 14, 16]. Exploiting the known anti-cancer properties of naturally occurring ITCs, we recently also reported on development of naphthalimide-isothiocyanate (NITC) compounds [15] with promising activity against melanoma. Several naphthalimide analogs with varying efficacy have been reported in literature as having promising anti-cancer activities [24-29]. Mitonafide, a naphthalimide analog and a well-known Topoisomerase-II α (Topo-II α) inhibitor, showed antitumor activity both preclinically [30] and in phase I and phase II clinical trials [31-33], but failed due to systemic toxicity issues [31-34]. We conducted a SAR study by introducing ITC (-N=C=S) functionality and altering the chain length to generate a series of NITC analogs that were effective in inhibiting melanoma tumor growth, while substantially reduced the systemic toxicity associated with mitonafide, resulting in more efficacious agents with higher therapeutic index. Our studies showed that the incorporation of -N=C=S functionality into mitonafide structure drastically reduced its systemic toxicity issues [15], possibly because of the enhanced reactivity of the compound towards glutathione and cysteine residues leading to the formation of conjugates that would excrete relatively faster from the body.

In the present study, we hypothesized that introducing the ISC (-N=C=Se) functionality of Akt pathway inhibitor ISC-4, into naphthalimide moiety, as in Topo-II α inhibitor mitonafide, would result in a dual Akt pathway/Topo-II α activity inhibitor with enhanced antitumor activity. Therefore, we synthesized a series of naphthalimide-ISC (NISC) compounds. In addition, since -N=C=Se follows similar mechanism as -N=C=S functionality [35], the new NISC compounds were also expected to have a similar safety profile as NITC compounds at effective doses, thus having a high therapeutic index. Furthermore, we also synthesized a series of naphthalimide analogs by incorporating a selenourea functionality in place of *N,N*-dimethyl in mitonafide, with or without nitro substitution to generate naphthalimide-selenourea (NSU) compounds. Both the NISC and NSU compounds were screened for their potency in inhibiting human melanoma cells viability, and the best identified compound, NISC-6 (**4d**), was evaluated for its anti-apoptotic activity on both BRAF^{V600E} mutant and BRAF^{WT} melanoma cells. Further, NISC-6's mechanism of action was characterized *in vitro*, and its tumor inhibitory activity was evaluated in melanoma xenograft mouse model.

2. Results and discussion

2.1. Design.

To create a dual inhibitor of Topo-II α and Akt signaling pathway, we intended to adapt a fragment based approach by blending -N=C=Se functionality of Akt pathway inhibitor ISC-4 and naphthalimide moiety of Topo-II α inhibitor mitonafide (**Figure 1**).

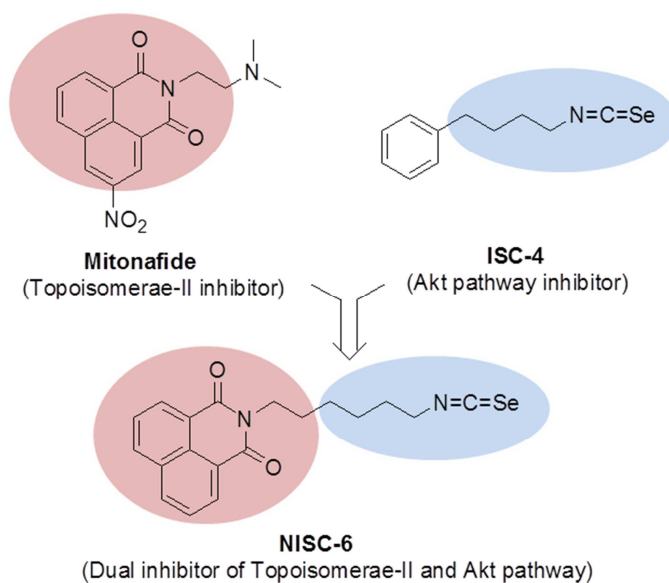


Figure 1. Fragment based design of dual inhibitor NSIC-6 using key functionalities of Mitonafide and ISC-4

In addition to this, we also took advantage of our previously published SAR results on NITC compounds. Two compounds, the NNITC-2 obtained by replacement of *N,N*-dimethylamino group of mitonafide by the $-N=C=S$ functionality, and NITC-6 obtained by extending the alkyl chain length to six carbons (**Figure 2**), were identified as the most potent agents that effectively inhibited melanoma cell viability, induced apoptosis, and inhibited tumor growth in a melanoma xenograft model [15]. The study also showed that increasing the alkyl chain length from 2 carbons (in NITC-2) to 6 carbons (in NITC-6), and substituting NITC-2 by a nitro group (as in NNITC-2) enhanced the potency of the compounds. Therefore, we first synthesized corresponding isosteric Se analogs, NISC-6 and NNISC-2, of the two NITC compounds (**Figure 2**). Interestingly, while the potency increased as expected in case of NISC-6, NNISC-2 was in fact less cytotoxic than NNITC-2. This suggested that unlike nitro substituted NNITC-2, which

was more potent than unsubstituted NITC-2, the nitro substitution at 3-position of naphthalimide ring system was not favorable in case of Se analogs. Therefore, we next focused on studying the chain length effect on unsubstituted NISC scaffold and synthesized compounds with two carbon (NISC-2) and four carbon (NISC-4) alkyl chains (**Figure 2**). However, in case of NISC analogs the increase in chain length did not seem to have a consistent contribution towards activity, although, NISC-6 with six carbon alkyl chain was identified as the most effective compound.

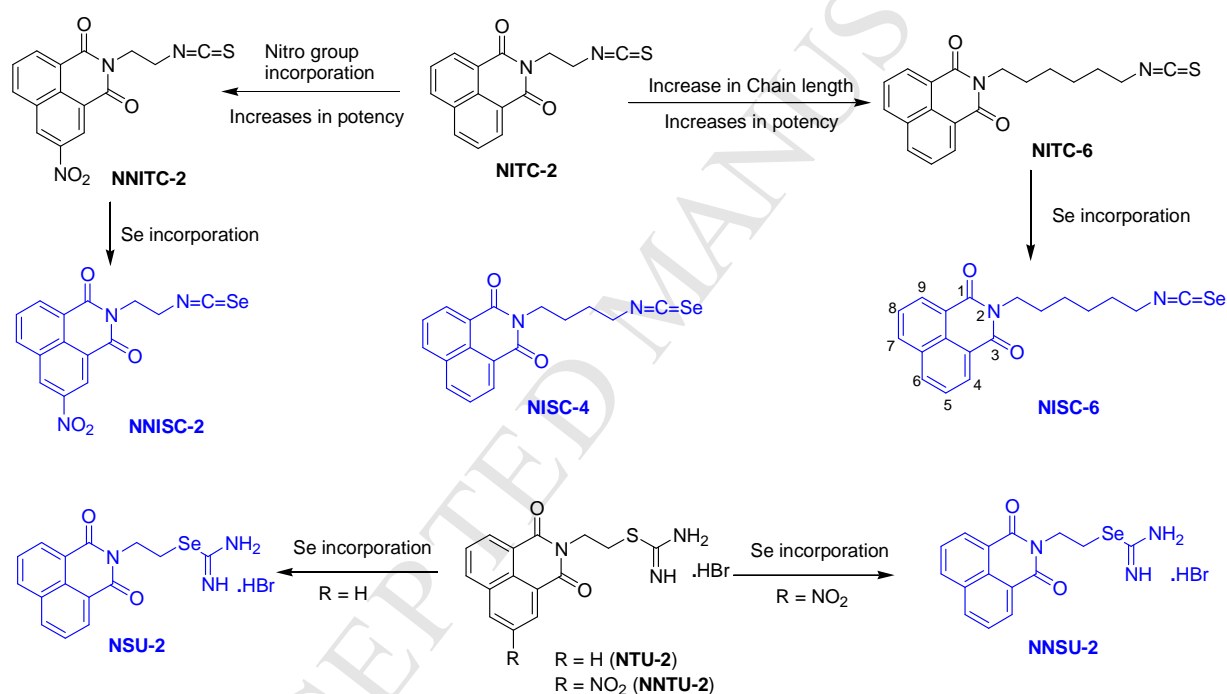


Figure 2. Rational designing of novel compounds.

Previously, we also synthesized naphthalimide-thiourea (NTU) analogs designed by in substituting *N,N*-dimethylamino group in mitonafide with a thiourea functionality, with or without

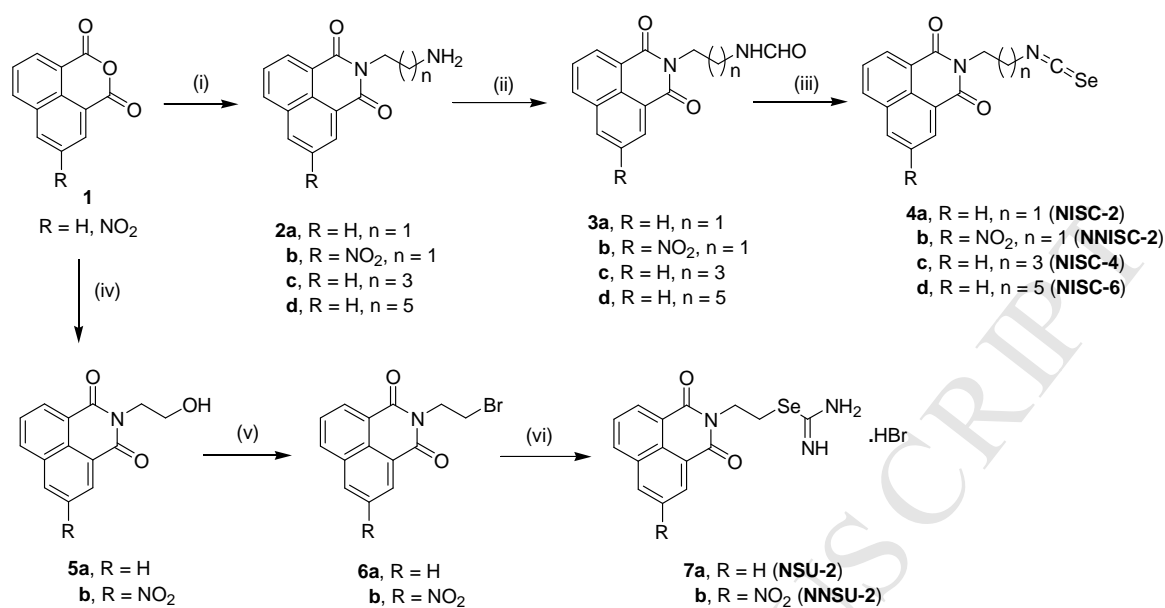
nitro substitution [15]. Although, NTU analogs [15] were less effective than the corresponding NITC compounds, literature reports have shown that selenourea functionality when incorporated into certain moieties in place of thiourea can significantly enhance the potency of the compound [36-38]. For example, isosteric Se analog of *S,S'*-1,4-phenylenebis(1,2-ethanediyl)bis-isothiourea (PBIT), a well-known chemopreventive agent that exerts its chemopreventive efficacy by inhibiting inducible nitric oxide synthase (iNOS) [39], by selenourea, as in PBISe [36, 38], significantly enhanced the cytotoxicity and tumor inhibitory action of the compound, particularly in melanoma xenograft models [36]. We have also recently shown various heterocyclic-selenoureas to be more potent anticancer agents than their corresponding thiourea analogs [37]. Therefore, to evaluate the effect of selenourea group when attached to a naphthalimide moiety, we also synthesized NSU compounds (**7a-b**) by replacing *N,N*-dimethylamino group in mitonafide by a selenourea functionality, with or without nitro substitution. Although, literature reports have shown potency to increase when thiourea functionality is replaced by selenourea in certain scaffolds [36-38], in the present case the NSU compounds were no better than their NTU counterparts.

2.2. Chemistry

The NISC compounds (**4a-d**) were synthesized as outlined in **Scheme 1** following our earlier reported method for phenylalkyl isoselenocyanates [13]. The key intermediates, aminoalkyl-naphthalimides **2a-d**, were synthesized by refluxing 1,8-naphthalic anhydride or 3-nitro-1,8-naphthalic anhydride with appropriate diaminoalkane following previously reported methods [15, 40, 41]. Formylation of compounds **2a-d** using ethyl formate and potassium carbonate under refluxing conditions gave formamides **3a-d**, which on treatment with

triphosgene and selenium powder in the presence of triethylamine in refluxing methylene chloride [13, 42] furnished the desired NISCs **4a-d** in good yields. The structural features for the formamides can be explained by taking specific example **3a**, which exhibited presence characteristic peaks for $-CHO$ at δ 7.94 (s, 1H) and $-NH$ at δ 8.14 (br s, 1H) as singlets in 1H NMR spectrum. Further in the ^{13}C NMR spectrum, the presence of carbonyl carbon of $-NH-CHO$ functionality at δ 164.1 ppm along with two carbonyl carbons of thalimide $-(C=O)_2N-$ functionality at δ 161.7 ppm supported the structure of the compound **3a**. In similar way, the structures of all other formamides **3b-d** were confirmed by 1H NMR, ^{13}C NMR and mass spectral analysis.

Similarly, the structural features of naphthalimide isoselenocyanates **4a-d** can be explained by taking specific example **4a**, which exhibited the absence of characteristic peak for $-NH$ (as in precursor compound **3a**) along with de-shielding of CH_2 protons attached to the $-N=C=Se$ functionality at δ 3.89 (t, 2H) as triplet integrating for two protons in 1H NMR spectrum. Further the presence of two nearly overlapping carbonyl carbons of naphthalimide $-(C=O)_2N-$ functionality at δ 164.06 and 164.02 ppm in the ^{13}C NMR spectrum confirmed the structure of the compound **4a**. The structures of isoselenocyanates **4b-d** were also confirmed based on 1H NMR, ^{13}C NMR and mass spectral analysis. It is interesting to note that while two naphthalimide carbonyl group peaks of compounds **3a** and **4a** as well as other symmetric analogs **3c,d** and **4c,d** overlap or nearly overlap, compounds **3b** and **4b** showed well separated carbonyl peak signals due to the presence of the nitro group.



Scheme 1. Synthesis of naphthalimide-isoselenocynate (**4**) and selenourea (**7**) derivatives.

Reagents and conditions: (i) diaminoalkane, EtOH, reflux, 2 h (ii) ethyl formate, K₂CO₃, reflux, 6 h (iii) thiophosgene, Se powder, Et₃N, CH₂Cl₂, reflux (iv) ethanolamine, EtOH, reflux, 1 h (v) PBr₃, EtOAc, 80 °C, 2 h (vi) selenourea, CH₃CN, reflux, 4 h.

The NSU compounds (**7a-b**) were synthesized as shown in **Scheme 1**. The precursor bromoalkyl naphthalimides **6a-b** were synthesized following our previously reported methods in two steps: refluxing 1,8-naphthalic anhydride or 3-nitro-1,8-naphthalic anhydride with ethanolamine in ethanol gave alcohols **5a-b** which on treatment with PBr₃ in refluxing ethyl acetate yielded compounds **6a-b**. The desired NSUs **7a** and **7b** were finally obtained by refluxing **6a-b** with selenourea in acetonitrile for 4 h. The compounds were purified by silica gel column chromatography and characterized on the basis of NMR and high-resolution MS. For example, ¹H NMR spectrum of **7a** exhibited the de-shielded protons of CH₂ functionality attached to isoselenouronium moiety at δ 3.54 (t, 2H) as triplet integrating for two protons. Further the presence of two carbonyl carbons of naphthalimide -(C=O)₂N- functionality at δ 167.4 and

164.0 ppm confirmed the structure of the compound **7a**. In similar way, the structure of other NSU compound **7b** was confirmed by ^1H NMR, ^{13}C NMR and mass spectral analysis.

2.3. Biology

2.3.1. Evaluation of the anti-proliferative activities of the novel molecules and SAR analysis

The effects of all the novel agents on cancer cell viability were evaluated using MTT assay. The compounds were screened in the four melanoma cell lines (human melanoma cells with BRAF^{V600E} mutation (UACC903, 1205Lu, and A375M) and cells having BRAF^{WT} (CHL-1)) at different concentration, in the range of 0 to 50 μM , and at 24, 48, 72 h time points. The precursor compound mitonafide, and clinically used BRAF^{V600E} inhibitor PLX-4032 were used as controls. **Table 1** lists the IC₅₀ for all the compounds in the four cell lines at three different time points. NISC compounds (**4a-d**) were in general more effective in inhibiting cell viability than the NSU derivatives (**7a-b**). Nitro substitution (compare NISC-2 vs. NNISC-2 and NSU-2 vs. NNSU-2) in fact reduced the potency of the compounds. This was in contrast to our previous report where nitro-substitution at 3-position of the naphthalimide ring enhanced the potency of the isosteric S analogs (NITC) of NISC compounds [15], suggesting that replacing S by Se can change the overall properties of the molecules. Furthermore, in previously published NITC compounds, the cytotoxicity increased with increasing alkyl chain length, while in the present case the chain effect was not consistent [15]. As indicated by **Table 1**, two compounds stood out as the most potent at reducing the cell viability, were NISC-2 and NISC-6, having the naphthalimide and isoselenocyanate moieties separated by 2 and 6 carbon alkyl chains, respectively. Considering

IC₅₀ values at different time points, NISC-6 was identified as the most effective compound. NISC-6 was more effective than PLX-4032 at early time point (24 h) in all cell lines tested (Table 1) and also exhibited a better potency at 48 and 72 h treatment in BRAF^{V600E} mutated UACC903 cells. In BRAF^{V600E} mutated 1205Lu and A375M cell lines, PLX-4032 was relatively more effective at 48 and 72 h treatment points. It is noteworthy that NISC-6 was ~15 times more effective in BRAF^{WT} CHL-1 cells compared to PLX-4032, indicating that NISC-6 was equally effective on both BRAF mutant and WT cells.

Table 1. Effect of novel compounds on different melanoma cancer cell lines.

		IC ₅₀ (μM)							
		NISC-2	NISC-4	NISC-6	NNISC-2	NSU-2	NNSU-2	Mitonafide	PLX-4032
1205Lu	24	11.0±0.1	13.1±1.4	13.4±2.5	21.6±2.3	46.8±8.6	>50	11.1±3.9	>50
	48	10.7±0.1	15.9±0.9	10.6±4.0	19.9±1.3	11.5±4.8	>50	0.9±0.1	7.6±1.6
	72	9.4±0.1	15.4±1.6	13.4±2.6	20.3±4.2	8.2±1.2	39.6±9.5	0.6±0.1	2.0±0.1
UACC903	24	6.3±0.0	13.1±1.4	13.4±2.5	21.6±2.3	46.8±8.6	>50	11.4±3.9	>50
	48	5.5±0.0	9.2±1.3	2.5±0.4	14.4±0.8	12.8±1.2	18.1±2.8	0.8±0.1	12.3±3.2
	72	5.9±0.0	12.0±1.3	1.7±0.3	15.9±2.5	12.1±1.5	14.0±1.9	0.5±0.0	2.7±1.00
A375M	24	9.7±1.2	19.4±1.4	11.8±2.1	24.8±1.3	>50	>50	3.8±0.4	>50
	48	7.8±0.4	21.0±1.6	2.7±0.4	21.0±0.8	17.9±2.9	>50	1.5±0.1	2.05±0.6
	72	8.0±0.9	28.4±5.4	4.4±0.5	24.0±3.7	28.7±9.1	25.8±4.5	1.3±0.1	0.5±0.2
CHL-1	24	6.3±0.3	9.7±1.3	13.7±2.9	15.3±0.0	17.9±3.8	>50	2.8±0.4	>50
	48	6.8±0.7	8.0±1.2	1.5±0.1	12.6±0.0	5.2±0.5	8.5±1.5	0.9±0.1	20.0±3.5
	72	7.6±0.5	8.9±1.4	0.8±0.0	11.0±3.2	5.1±0.0	13.5±1.6	0.5±0.0	12.7±1.9

Data represent mean IC₅₀ values (± SD) of % cell viability determined by the MTT assay in triplicates. IC₅₀ values were obtained by performing non-linear regression (variable slope) analysis using GraphPad Prism.

Figure 3A shows the cell viability curves for NISC-6 in UACC903 cell line at 24, 48, and 72 h time points. Comparison of NISC-6 with its precursor compounds, mitonafide and ISC-4, revealed that NISC-6 was more cytotoxic than ISC-4 but was slightly less effective than

mitonafide (**Figure 3B**). Since our goal was also to make the compound more tolerable than mitonafide, we compared the effects of NISC-6 with mitonafide on normal cells viability. Human dermal fibroblast cells (nHDFs) were used as the representative normal cells. Effect of NISC-6 and mitonafide on viability of nHDFs was evaluated using MTT assay. As represented by the bar graph in **figure 4**, at the concentration of 2.5 and 5 μM , NISC-6 showed more than 70% viable nHDF cells, while mitonafide showed less than 20% viable cells. Overall, this data indicate that although NISC-6 is relatively less potent, it is more tolerable than mitonafide, and is more selective towards cancer cells than normal cells.

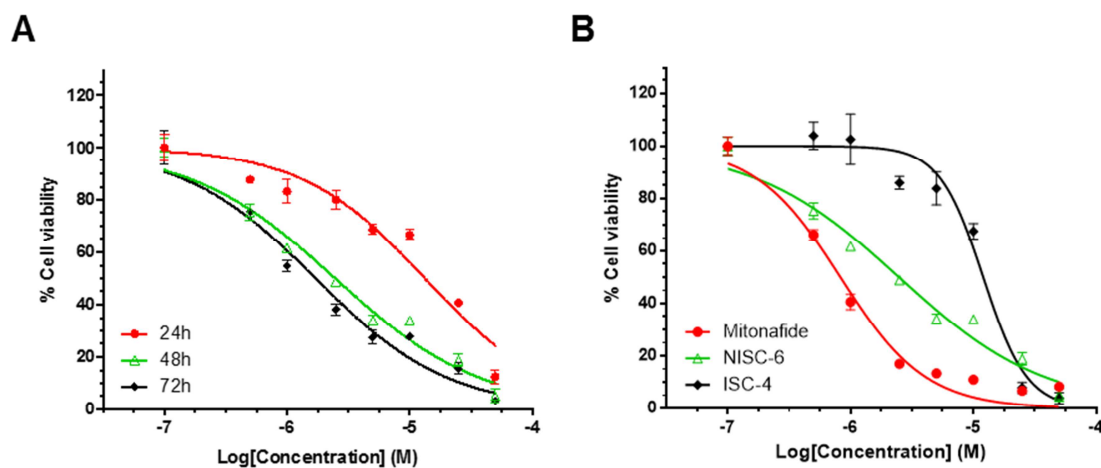


Figure 3. NISC-6 potently inhibited cell viability of melanoma cells. (A) Melanoma cells (UACC903) were treated for 24, 48 and 72h at different concentrations of NISC-6. MTT assay was performed as described in Method and Material section. Cell viability curves were obtained by performing non-linear regression using GraphPad Prism software. Calculated IC_{50} for all the time points are shown in Table 1. (B) All three compound (NISC-6, ISC-4 and Mitonafide) were treated for 48h and growth curves were obtained in a similar manner as (A).

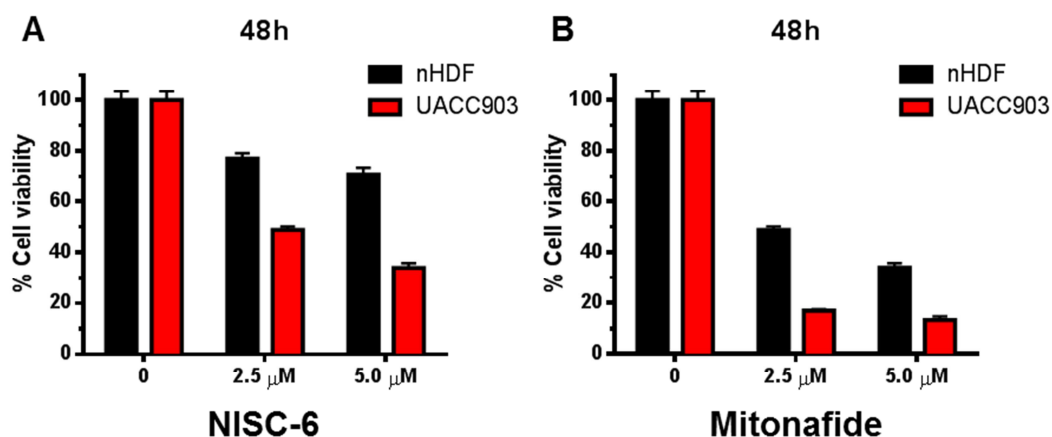


Figure 4. NISC-6 is more tolerable than Mitonafide in normal fibroblast cells, while at the same time effective on cancer cells. Melanoma cells (UACC903) and normal human fibroblasts (nHDFs) were treated for 48h at given concentrations of NISC-6 and mitonafide. MTT assay was used to measure cell viability. Bar graph represents mean \pm SD.

2.3.2. Molecular docking study of NISC-6 in the active sites of Akt and Topo II α

NISC-6 was designed to be a dual inhibitor of Topo-II α activity and Akt signaling pathway. In order to afford some guidance for its design, *in silico* docking simulations were conducted using the CDOCKER algorithm [43] in Discovery Studio (DS) program. NISC-6 was docked into both Akt1 and Topo-II α structures and compared with ISC-4 and mitonafide, respectively. Prior to docking these compounds, the re-docking of the co-crystallized ligand into the binding site of each protein was conducted to check the predictive efficiency of the docking protocol. For this purpose, the native ligands, EVP1 (etoposide) and XM11 were docked with Topo-II α and Akt1, respectively, and their best poses were identified based on the scoring function (-CDOCKER energy). The predicted docking pose and its X-ray structure showed a very good structural correlation (Figure S1a-b, Supplementary Material) based on the favorable computed root mean square deviation ($< 1\text{\AA}$). Moreover, the predicted poses displayed interactions with similar amino acid residues of Akt1 (Glu234, Arg4) and Topo-II α (Arg503, DG13, Asp479, DA12) as observed

in their native ligands, and thus validated the reproducibility efficiency of the protocol. NISC-6 (**4d**) and the reference compounds were subsequently docked into the binding sites of Akt1 and Topo-II α (details in method section) using the same docking protocol (Figure 5). The computed negative binding energies (BEs) suggested the tendency of each compound to inhibit the proteins under investigation. NISC-6 (BE = -76.7 kcal mol⁻¹) was found to be the stronger inhibitor of Topo-II α than mitonafide (BE = -37.8 kcal mol⁻¹). NISC-6 (BE = -63.7 kcal mol⁻¹) also exhibited stronger interaction with Akt1 as compared to ISC-4 (BE = -27.4 kcal mol⁻¹). NISC-6 thus demonstrated stronger interactions with both Akt1 and Topo-II α as compared to the reference controls ISC-4 and mitonafide, respectively, and therefore promise to be a potent dual inhibitor.

The ligand-protein complexes visualized further to understand their binding modes revealed the predominance of electrostatic and hydrophobic forces accounting for their host-guest relationship. NISC-6 (**Figure 5A**), for instance, exhibited electrostatic interactions with Asp292 (cation- π) and Lys179 (anion- π), a hydrophobic interaction (π - π stacking) with Phe161 and a non-classical hydrogen bond (2.6 Å) with Glu234 of Akt1 protein. ISC-4 in contrast missed all those interactions observed in case of NISC-6 and mitonafide, and displayed only hydrophobic (π - π stacking) interaction with Phe442 through its phenyl ring (**Figure 5B**).

In case of Topo-II α , NISC-6 (**Figure 5C**) fitted nicely into the binding cavity *via* two non-classical hydrogen bonds (2.98 Å, 2.99 Å) with Arg503 through its alkyl moiety (-CH₂-) and multiple hydrophobic interactions (π - π stacking and π -alkyl) with the guanine (DG13) and adenine (DA12) nucleotides. Mitonafide exhibited hydrophobic forces with cytosine (DC8), thymine (DT9) and guanine (DG13) nucleotides of topo-II in addition to two non-classical hydrogen bonds with Leu502 (Figure 5D). The nitro group of mitonafide was also found to be engaged in electrostatic interaction with the adenine (AD12) nucleotide. Although, both the

NISC-6 and mitonafide showed good binding affinity for topo-II, the binding conformation of the former was observed to be more folded resulting in its tighter fitting into the binding groove of the protein and in turn more stability of its complex ($BE = -76.7 \text{ kcal mol}^{-1}$) relative to the latter. Furthermore, the NISC-6 displayed interactions with similar amino acids as observed in case of etoposide (Arg503, DG13), and suggested that this compound could probably inhibit the enzyme by same mechanism as etoposide. Overall, the docking results suggest that the aromatic ring system present in NISC-6 is vital for locking its geometry in the binding site of both the proteins.

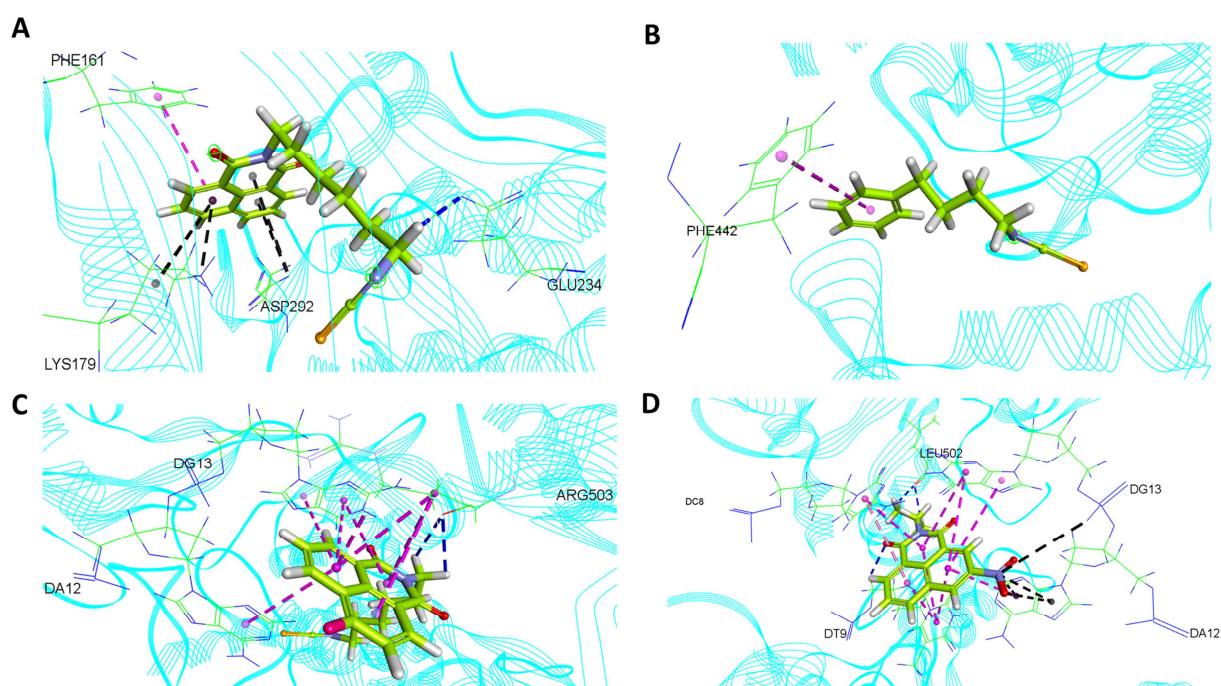


Figure 5. NISC-6 docks into the binding pockets of both Akt and Topo-II α . Docked pose of NISC-6 (A) and ISC-4 (B) into the binding cavity of Akt1. Docked pose of NISC-6 (C) and mitonafide (D) into the binding cavity of Topo-II α . Ligand poses are shown in sticks (lemon color), while the protein residues are shown in line ribbon (sky blue) format. Interacting amino acids of protein as green lines, non-classical hydrogen bonds as blue dotted lines, electrostatic interactions as black dotted lines and hydrophobic interactions are shown as magenta dotted lines.

2.3.3. NISC-6 inhibited *in vitro* Topo-II α activity and phosphorylation of Akt.

Based on structural design, NISC-6 possesses both the active site of ISC-4 and mitonafide, which are the Akt pathway and Topo-II α activity inhibitors, respectively. Our docking studies showed that NISC-6 is able to fit in the active sites of both the proteins, more strongly than the parent molecules. In order to prove the dual inhibitory property of NISC-6 experimentally, we first tested the effect NISC-6 on Topo-II α activity, *in vitro*. Topo-II α enzyme, can convert supercoiled DNA into relaxed DNA strands. Hence, using these principle, we tested NISC-6's ability to inhibit Topo II α activity *in vitro*. Purified Topo II α enzyme was incubated with super coiled DNA in presence of DMSO, NISC-6, mitonafide or etoposide. Mitonafide and etoposide were used as positive controls. As shown in figure 6A, super coiled DNA ran faster than relaxed DNA strand or opened circular DNA, followed by relaxed DNA strand and Nicked open DNA. In the presence of just the enzyme and supercoiled DNA, almost all the super coiled DNA was converted into nicked open DNA. However, in presence of the positive control, increasing dose of etoposide or mitonafide, the super coiled DNA is not converted in to nicked open DNA. Similar results were observed for NISC-6, which showed very similar response as mitonafide at inhibiting Topo-II α activity.

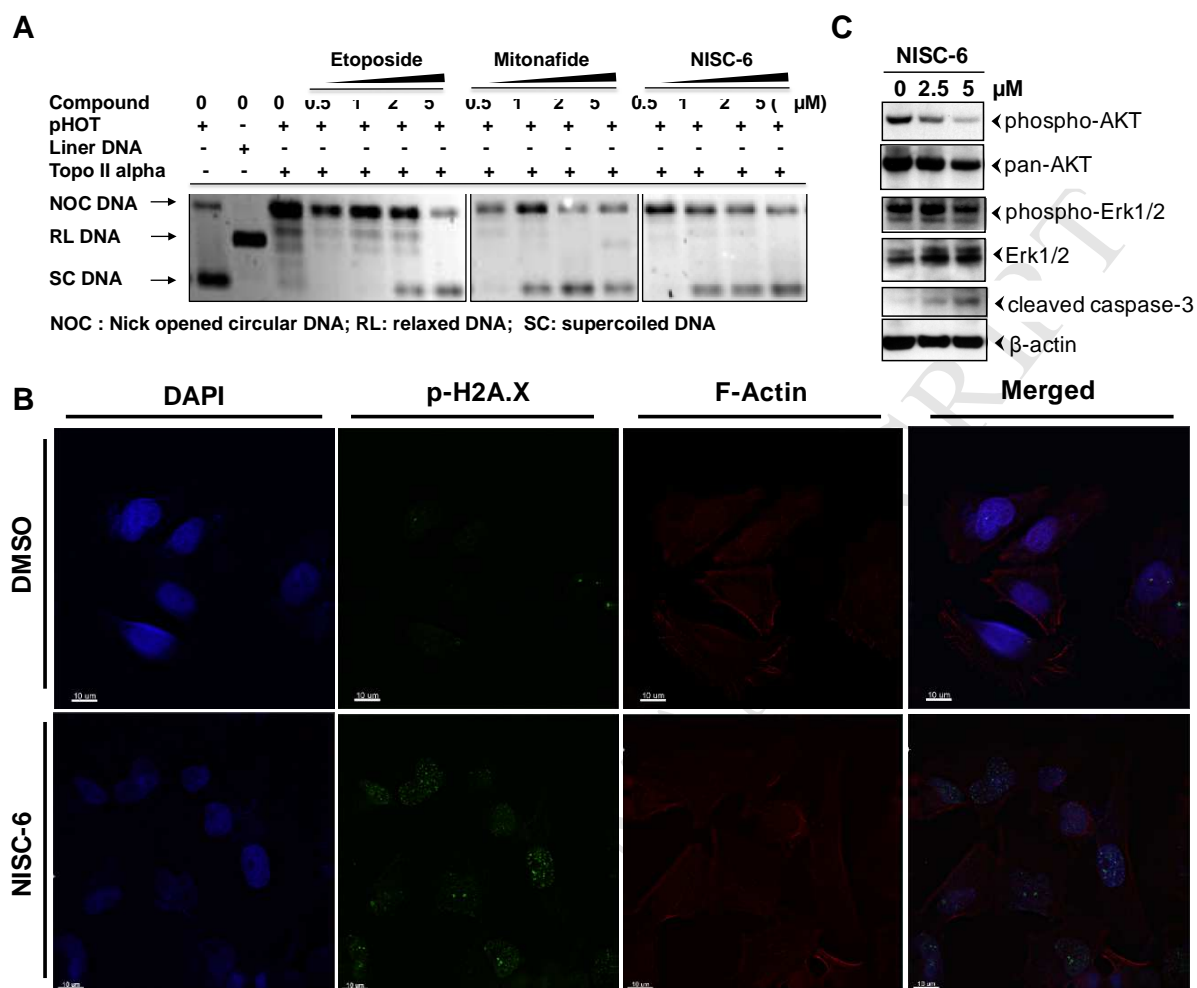


Figure 6. NISC-6 inhibited TopoII α activity in vitro and also inhibits p-AKT levels in melanoma cells. (A) NISC-6 inhibits Topo II α from relaxing the supercoiled plasmid. In brief, pBR322 plasmid DNA was incubated with Topo-II α in presence of different drug concentration, along with reaction mixture for 1 h at 37 °C. After incubation, the samples were subjected to gel electrophoresis on 1% agarose gel. Gel was stained with ethidium bromide for visualizing the DNA bands. **(B)** UACC903 cells were treated with NISC-6 at given concentration for 24 h. Whole cell lysates were subjected to Western blot analysis. Resulting blots were probed with phospho-Akt and pan-Akt. β -actin was used as loading control. **(C)** NISC-6 increase DNA damage marker, p-H2A.X, expression in melanoma cells. UACC 903 cells were seeded on a glass coverslip and treated with NISC-6 (5 μ M) for 6 h. After treatment, cells were fixed and probed with anti-body against p-H2A.X. DAPI (blue) was used to stain the nucleus and phalloidin (red) was used to stain F-actin.

It is very well established that phosphorylation of histone H2A.X is indicative of DNA damage, particularly in case of DNA double strand breaks [44]. Further, Topo-II inhibitors are known to increase p-H2AX expression [45]. Since, NISC-6 inhibited Topo-II α activity, we evaluated its ability to increase p-H2A.X expression in UACC 903 cells. Phospho-H2A.X (DNA damage marker) expression increases upon DNA damage by external agents or by apoptosis (cell death). However, DNA damage by Topo-II α inhibitors is an early event compared to apoptosis [46]. Therefore, we investigated the levels of p-H2A.X at early time point of 6 h rather than 24 h. As shown in **figure 6B**, p-H2A.X expression increased when cells were incubated with 5 μ M dose of NISC-6, compared to the vehicle control. This finding further confirmed that NISC-6 induces DNA double strand breaks by inhibiting Topo-II α activity.

To test the potential of NISC-6 to inhibit the phosphorylation of Akt, UACC903 cells were treated with increasing dose of NISC-6 for 24 h and phosphorylation of Akt was observed using Western blot. NISC-6 potently inhibited phosphorylation of Akt in a dose dependent manner (**Figure 6C**). p-Erk was not affected showing specificity. Results obtained from both the Topo II α activity assay and Western blot analysis of p-Akt, along with our docking studies strongly suggest that NISC-6 possesses both the Topo-II α inhibitory activity and ability to inhibit Akt pathway as per the structural design.

2.3.4. NISC-6 induced apoptotic cell death in melanoma cells.

Since both the Topo-II α and Akt are well-known markers of resistance towards cancer cell death and have been associated with poor prognosis in clinic [47, 48], we wanted to see whether the dual inhibition of Topo-II α and Akt pathway by NISC-6 translates to apoptotic cell death.

Hallmark of apoptosis is the activation of caspase 3/7 and presence of phosphatidylserine (PS) on the outer surface of the plasma membrane [49]. Based on our MTT data, we selected two doses of NISC-6 to treat UACC903 cells for 24 h. Treated cells were tested for the presence of PS on the outer leaflet of plasma membrane by annexin-V staining, and presence of caspase 3/7 activity. This was achieved by using Muse Live & Dead kit, and Caspase 3/7 activity kit. Both the kits contain 7-AAD, which can only enter the cells when plasma membrane has lost its integrity. Therefore, if the cells are dying in a necrotic manner, they will be stained only with 7-AAD. Muse Live & Dead kit contains annexin-V dye which cannot enter intact cells and can only bind to PS on the outer leaflet of the plasma membrane, while caspase 3/7 activity kit contains a molecule which can travel freely inside the cells and fluoresce only when cleaved in presence of active caspase 3/7. The fluorescence present in both kits can then be detected via MUSE cell analyzer. **Figure 7A-B** shows the graphs obtained from Muse cell analyzer. The bottom left corner of the graph represents healthy live cells (Annexin-V negative, Casapse 3/7 negative, 7-AAD negative), bottom right corner represents early apoptotic cells (Annexin-V positive, Casapse 3/7 positive, 7-AAD negative), top right corner represents late apoptotic cells (Annexin-V positive, Casapse 3/7 positive, 7-AAD positive) and top left corner represents necrotic cells (Annexin-V negative, Casapse 3/7 negative, 7-AAD positive). As shown in **figure 7A-B**, increasing dose of NISC-6 translocated the cells from bottom left corner to bottom right corner to top right corner in a dose dependent manner. There were no cells present in top left corner at the doses tested, indicating that treatment with NISC-6 does not induce necrosis. It is clear from **figure 7A-B**, that NISC-6 dose dependently increases apoptosis in melanoma cells. Taken together, it can be concluded that NISC-6 induces cells death in an apoptotic manner.

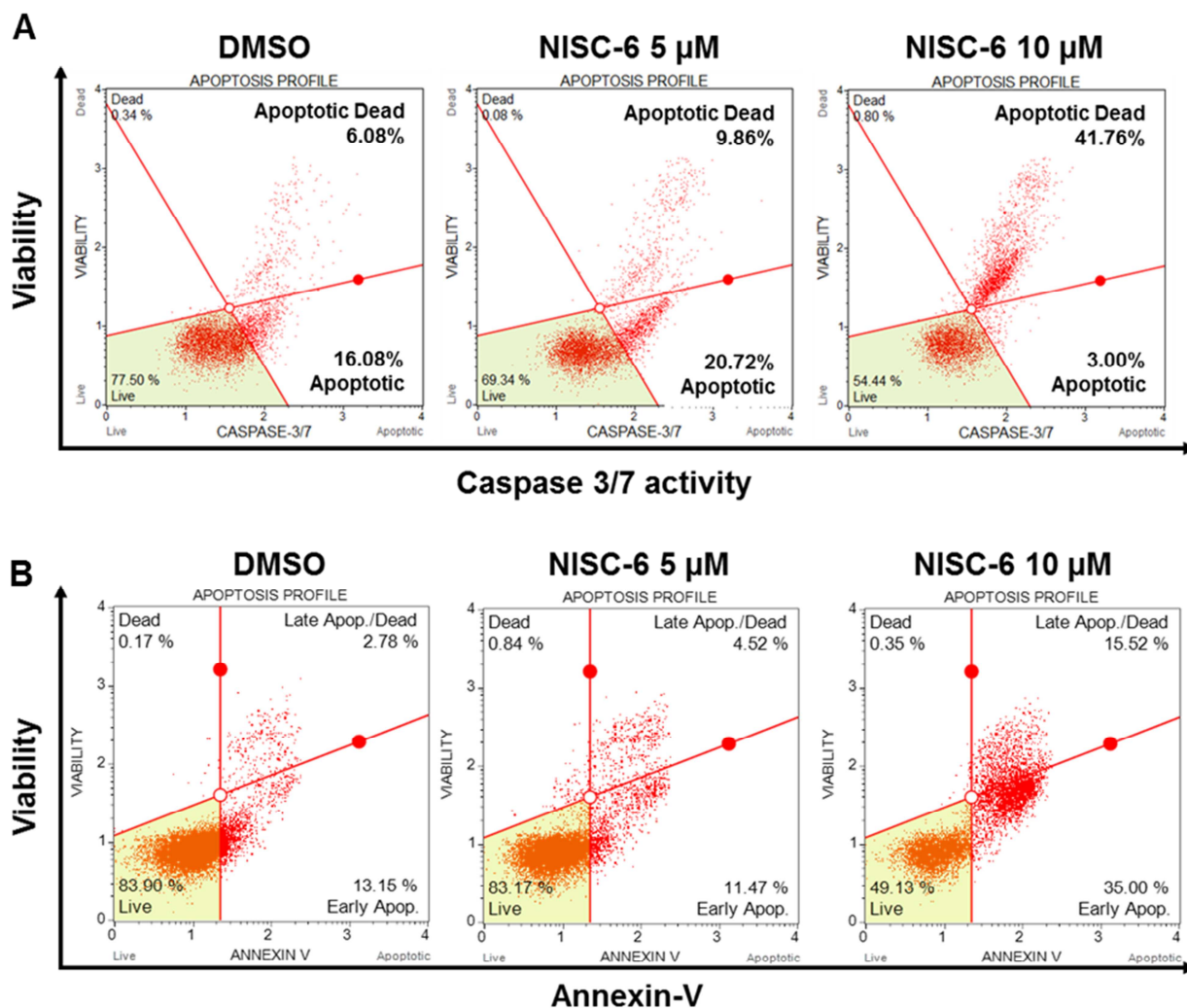


Figure 7. NISC-6 induced apoptotic cell death melanoma cells. Melanoma cells (UACC903) were treated with NISC-6 for 24 h at given concentrations. At the end of the experiment, cells were subjected to (A) Caspase 3/7 activity assay and (B) Annexin-V (Live and Dead) assay using a Muse cell analyzer. Performing the assay as described in the methods section, generated a histogram as shown above. Bottom left corner represents live cells (Caspase 3/7 (-), Annexin-V (-) and 7-AAD (-)), bottom right corner represents early apoptotic cells (Caspase 3/7 (+), Annexin-V (+) and 7-AAD (-)), top right corner represents late apoptotic cells (Caspase 3/7 (+), Annexin-V (+) and 7-AAD (+)) and top left corner represents necrotic cells (Caspase 3/7 (-), Annexin-V (-) and 7-AAD (+)).

2.3.5. NISC-6 inhibited tumor growth in a melanoma xenograft mouse model.

NISC-6 effectively inhibited both Topo-II α activity as well as phosphorylation of Akt, and induced apoptotic cancer cell death in melanoma cells. To determine if the in vitro efficacy of NISC-6 translates to in vivo models, we performed tumor inhibition studies in xenograft mouse model of melanoma. Athymic nude mice were subcutaneously injected with UACC 903 cells and tumor development was allowed to occur for six days, by which time tumors undergo vascularization (angiogenesis). Mice were then injected i.p with NISC-6 or control DMSO, three times a week on Mondays, Wednesdays and Fridays at a dose of 0.6 μ mole in DMSO (100 μ L). Tumor size was measured periodically and at the same time animal weights were also measured. As shown in figure 8A, NISC-6 inhibited tumor growth and by the end of the experiment (40th day) it was able to reduce tumor burden by ~69% as compared to vehicle treated mice (Mean \pm SEM). These results complimented our in vitro cell viability and apoptosis assays data. Body weight loss is often used as a measure of drug-induced toxicity. No evidence of systemic toxicity was observed at the dose used as evidenced by the body weights; NISC-6 treated mice did not show any significant weight loss as compared to the vehicle treated mice (**Figure 8B**). Hence, tumor inhibition along with in vitro results strongly suggest the potential of NISC-6 as a novel dual targeting therapy for melanoma.

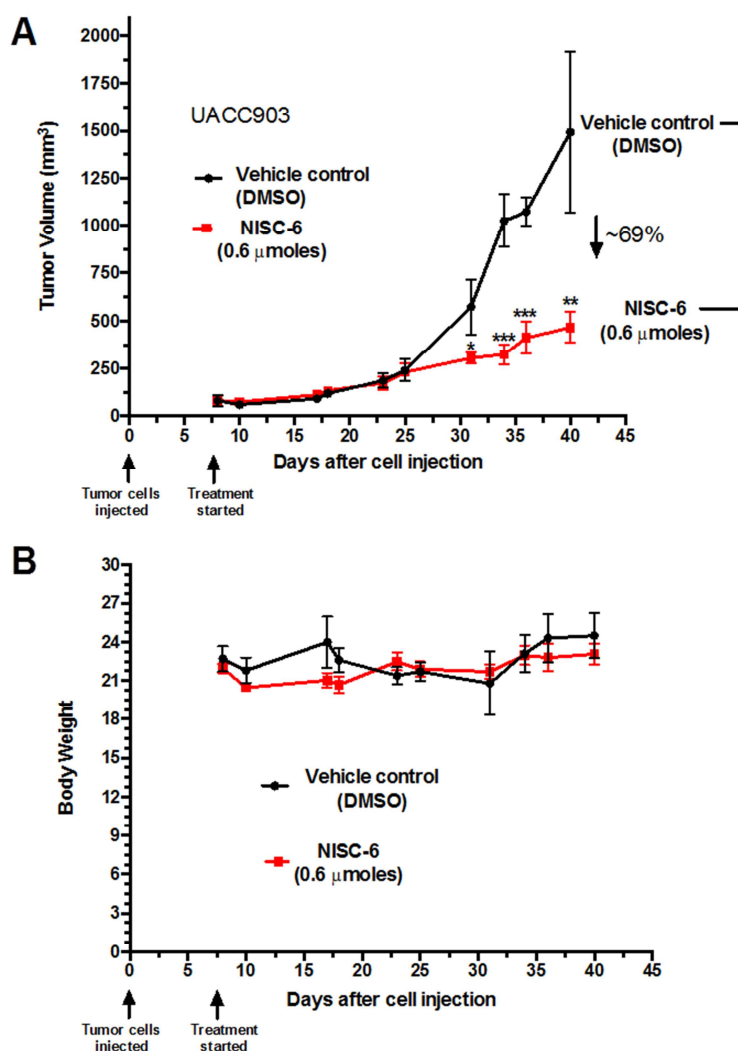


Figure 8. NISC-6 potently inhibited melanoma tumor growth in athymic nude mice (A) Six days after subcutaneous injection of UACC 903 melanoma cells, nude mice were treated i.p. with DMSO or NISC-6 (0.6 μ moles) thrice per week. NISC-6 significantly reduced tumor growth (~69%) compared to DMSO control. **(B)** Body weights of treated mice compared to the control DMSO vehicle treated mice showed no significant differences between groups. Data represents the mean tumor volume or body weight with error bars representing SEM.

2.3.6. Computation of physiochemical properties of NISC-6

NISC-6 promises to be an efficacious and safe drug candidate to develop further since it effectively killed melanoma cells while being non-toxic to normal cells, and reduced tumor growth *in vivo* without any apparent systemic toxicity. Our *in vivo* results further suggest that NISC-6 must be bioavailable to reduce tumor growth so effectively. However, to assess its drug likeness, we computed its physiochemical and ADME (Absorption, Distribution, Metabolism and Extraction) properties. The knowledge of physicochemical and ADME properties of prospective drug candidates is crucially important in the drug design programs. The Lipinski's "rule of five" has widely been employed to filter the chemical entities, which have potential of acting as drugs [50, 51]. According to this rule, any scaffold with the molecular weight (MW) greater than 500, hydrogen bond donors (HBDs) more than five, hydrogen bond acceptors (HBAs) more than 10 and an octanol-water partition coefficient (logP) value more than 5, is likely to have poor permeation or absorption under physiological conditions. Therefore, the non-compliance of any one of these rules may lead to the poor bioavailability of the compound of interest. In order to check the drug-likeness of NISC-6, we subjected it to the analysis of Lipinski (or Pfizer) rule of five. Computation was performed using the "Filter by Lipinski and Veber rule" algorithm embedded in DS 4.0 Client. The predicted Lipinski's properties of NISC-6, for instance, MW; 385, HBDs; 0, HBAs; 4 and LogP; 3.2, exhibited excellent compliance with the Lipinski's rule of five, and favored the tendency of this compound to act as a drug physiologically. Finally, the topological polar surface area (TPSA), which is another very useful property to measure the hydrogen bonding capability of compounds, was computationally predicted using the same tool in DS. Any compound with $TPSA < 140 \text{ \AA}^2$ is considered to have

high oral availability [52, 53]. The computed TPSA of value 49.7 \AA^2 for NISC-6 also supported its drug-likeness.

3. Conclusion

Novel naphthalimide analogs bearing isoselenocyanate (**4a-d**) and selenourea (**7a-b**) functionalities have been developed using a fragment-based design. Both, NISC (**4a-d**) and NSU (**7a-b**) analogs exhibited efficient inhibition of melanoma cell growth, NISC compounds showed relatively better potency. Based on cell viability assays in BRAF^{V600E} mutant and BRAF^{WT} human melanoma cells, NISC-6 was identified as the most effective compound that was toxic to cancer cells while sparing the normal nHDF cells. As expected from its fragment-based design, incorporating naphthalimide moiety of Topo-II α inhibitor mitonafide and ISC moiety of Akt pathway inhibitor ISC-4, NISC-6 was found to be a dual inhibitor of Topo-II α and Akt pathway as evidenced by both the docking studies and the experimental results. However, more in-depth mechanistic studies would be required to establish whether these are the real targets of NISC-6 or are inhibited as a consequence of some upstream target(s). NISC-6 was effective in inducing apoptosis in human melanoma cells and effectively inhibited subcutaneous melanoma tumor growth (~69%) without any apparent systemic toxicity. NISC-6 thus seems to be a promising drug candidate to develop further as a potential melanoma therapeutic.

4. Experimental

4.1. Chemistry

4.1.1. General

Melting points were recorded on a Fischer-Johns melting point apparatus and are uncorrected. $^1\text{H-NMR}$ and $^{13}\text{C-NMR}$ spectra were recorded on a Bruker Advance 500 instrument in either D_2O or CDCl_3 , operating at 500 and 125 MHz, respectively. Chemical shifts are reported in δ values (ppm) and J values are reported in hertz (Hz). The signals are quoted as s (singlet), d (doublet), t (triplet), q (Quartet), m (multiplet), and dd (doublet of doublet). High resolution (ESI or EI) MS were carried out at the Chemistry Instrumentation Center, State University of New York at Buffalo, NY. Experiments involving moisture and/or air sensitive components were performed under a nitrogen atmosphere in oven-dried glassware. Reagents, starting materials, and anhydrous solvents were purchased from commercial suppliers and were used as received. Reaction courses were monitored by thin-layer chromatography (TLC) on pre-coated silica gel 60 F₂₅₄ aluminum sheets (Merck, Darmstadt, Germany), and the spots were visualized under UV light. The crude reaction products were purified by silica gel column chromatography using silica gel 60 Å (Merck, 230-400 mesh). The mitonafide was synthesized following a literature method [41]. Naphthalimide linked alkylamines (**2a-d**) [40, 54], alcohols (**5a,b**) and bromide (**6a,b**) [55] were synthesized using reported methods [15]. The purity of the final compounds ($\geq 97\%$) was quantified by analytical high performance liquid chromatography analysis by comparing the peak areas of the product relative to any impurities.

4.1.2. General method for synthesis of naphthalimide-alkyl formamides. Formamides (**3a-d**) were synthesized following a literature method [56].

4.1.2.1. 2-(2-Formamido-ethyl)-benzo[de]isoquinoline-1,3-dione (3a).

Ethyl formate (3.1 g, 41.7 mmol) was added dropwise to a mixture of naphthalimide alkylamine **2a** (1.0 g, 4.2 mmol) in ethanol (10 mL) at room temperature and the resulting mixture was heated at 60 °C for 18 h. The solvent was removed under reduced pressure to yield the

corresponding naphthalimide-alkylformamide **3a** as a crude product which was purified by crystallization from a mixture of CH₂Cl₂:hexanes (9:1) to yield 0.7 g (62.5%) as pale yellow solid, m.p. 163–165°C. ¹H NMR (500 MHz, DMSO-*d*₆): δ 3.45 (m, 2 H, CH₂NH), 4.17 (t, 2 H, *J* = 6.0 Hz, CH₂N), 7.87 (t, 2 H, *J* = 7.5 Hz, Ar-*H*₅,*H*₈), 7.94 (s, 1 H, CHO), 8.14 (br s, 1H, NH), 8.45 (d, 2 H, *J* = 8.0Hz, Ar-*H*₆,*H*₇), 8.49 (d, 2 H, *J* = 7.0 Hz, Ar-*H*₄,*H*₉); ¹³C NMR (125 MHz, DMSO-*d*₆) δ 164.1 (C=O), 161.7 (2 × C=O), 134.7, 134.6, 131.7, 131.16, 131.11, 127.9, 127.6, 122.6 (aryl), 39.2 (NCH₂), 35.5 (CH₂NH); HRMS (EI) *m/z* calcd for C₁₅H₁₂N₂O₃, 268.0842; found: 268.08514.

4.1.2.2. 3-Nitro[2-(2-formamido-butyl)]-benzo[de]isoquinoline-1,3-dione (**3b**).

Ethyl formate (2.55 g, 34.4 mmol) was added dropwise to a mixture of naphthalimide alkylamine **2b** (1.0 g, 3.44 mmol) in ethanol (10 mL) at room temperature and the resulting mixture was heated at 60 °C for 18 h. The solvent was removed under reduced pressure to yield the corresponding naphthalimide-alkylformamide **3b** as a crude product which was purified by crystallization from a mixture of CH₂Cl₂:hexanes (9:1) to yield 0.6 g (56.0%) as yellow solid, m.p. 215–217°C. ¹H NMR (500 MHz, DMSO-*d*₆): δ 3.47 (m, 2 H, CH₂NH), 4.19 (t, 2 H, *J* = 6.0 Hz, CH₂N), 7.9 (1H, s, CHO), 8.07 (t, 1 H, *J* = 7.5 Hz, Ar-*H*₈), 8.10 (br s, 1 H, NH), 8.70 (d, 1 H, *J* = 7.0 Hz, Ar-*H*₇), 8.78 (d, 1 H, *J* = 7.5 Hz, Ar-*H*₉), 8.97 (d, 1 H, *J* = 2.5 Hz, Ar-*H*₄), 9.49 (d, 1 H, *J* = 2.0 Hz, Ar-*H*₆); ¹³C NMR (125 MHz, DMSO-*d*₆) δ 163.4 (C=O), 163.0 (C=O), 161.9 (C=O), 146.3, 136.7, 134.3, 131.3, 130.1, 130.0, 129.7, 124.5, 123.2, 123.1 (aryl), 39.5 (NCH₂), 35.4 (CH₂NH); HRMS (EI) *m/z* calcd for C₁₅H₁₁N₃O₅, 313.0693; found: 313.06946.

4.1.2.3. (2-Formamido-butyl)-benzo[de]isoquinoline-1,3-dione (**3c**).

Ethyl formate excess (2.7 g, 37.3 mmol) was added dropwise to a mixture of naphthalimide alkylamine **2b** (1 g, 3.7 mmol) in ethanol (10 mL) at room temperature and the resulting mixture was heated at 60 °C for 18 h. The solvent was removed under reduced pressure to yield the corresponding naphthalimide-alkylformamide **3c** as a crude product. This was purified by crystallization from CH₂Cl₂/hexanes 9:1 to yield 0.75 g (68.8%) as pale brown solid, m.p. 160–162 °C. ¹H NMR (500 MHz, DMSO-*d*₆): δ 1.46-1.51 (m, 2 H, CH₂), 1.62- 1.67 (m, 2 H, CH₂), 4.27 (m, 2 H, , CH₂NH), 4.05 (t, 2 H, *J* = 6.5 Hz, CH₂N), 7.86 (t, 2 H, *J* = 6.5 Hz, Ar-*H*₅,*H*₈), 7.98-7.99 (m, 2 H, NH, CHO), 8.44 (dd, 2H, *J* = 8.0, 1.0 Hz, Ar-*H*₆,*H*₇), 8.49 (dd, 2 H, *J* = 7.5, 1.0 Hz, Ar-*H*₄,*H*₉); ¹³C NMR (125 MHz, DMSO-*d*₆) δ 163.9 (C=O), 161.40 (C=O), 161.38 (C=O), 134.7, 131.7, 131.2, 127.8, 127.6, 122.5 (aryl), 41.0 (NCH₂), 37.2 (CH₂NH); 26.9 (CH₂), 25.6 (CH₂); HRMS (EI) *m/z* calcd for C₁₇H₁₆N₂O₃, 296.1155; found: 296.11569

4.1.2.4. 2-(2-Formamido-hexyl)-benzo[de]isoquinoline-1,3-dione (**3d**).

Ethyl formate excess (2.5 g, 33.7 mmol) was added to a mixture of naphthalimide alkylamine **2d** (1.0 g, 3.4 mmol) in ethanol (10 mL) at room temperature and the resulting mixture was heated at 60 °C for 18 h. The solvent was removed under reduced pressure to yield the corresponding naphthalimide-alkylformamide as a crude product. This was purified by column chromatography from CH₂Cl₂/hexanes 7:3 to yield 0.6 g (54.5%) as pale yellow solid, m.p. 129–131 °C. NMR (500 MHz, DMSO-*d*₆): δ 1.50-1.30 (m, 6 H, CH₂CH₂CH₂), 1.65-1.60 (m, 2H, CH₂), 3.10-3.05 (m, 2 H, CH₂NH), 4.05 (t, 2 H, *J* = 7.5 Hz, CH₂N), 7.85 (t, 2 H, *J* = 7.5 Hz, Ar-*H*₅,*H*₈), 8.00-7.95 (m, 2 H, NH and CHO), 8.43 (d, 2 H, *J* = 8.0 Hz, Ar-*H*₆,*H*₇), 8.48 (d, 2 H, *J* = 7.0 Hz, Ar-*H*₄,*H*₉); ¹³C NMR (125 MHz, DMSO-*d*₆) δ 163.8 (C=O), 161.3 (2 × C=O), 134.7, 131.7, 131.1, 127.7,

127.6, 122.5 (aryl), 41.2 (NCH₂), 37.4 (CH₂NH); 29.3 (CH₂), 27.9 (CH₂); 26.6 (CH₂), 26.5 (CH₂); ESIMS *m/z* 325 (M+H)⁺.

4.1.2.5. 2-(2-Isoselenocyanato-ethyl)-benzo[de]isoquinoline-1,3-dione (4a).

To a refluxing mixture of **3a** (0.15 g, 0.56 mmol), triethylamine (0.19 g, 1.87 mmol), and 4 Å molecular sieves in CH₂Cl₂ (10 mL), was added dropwise a solution of triphosgene (0.07 g, 0.23 mmol) in CH₂Cl₂ (5 mL) for a period of 1 h. After the addition was complete, the mixture was refluxed for an additional 2 h. Selenium powder (0.5 g, 0.94 mmol) was then added, and the resulting mixture was refluxed for an additional 30 h. The mixture was cooled and filtered, and the solvent was evaporated to yield the crude mixture, which was purified by silica gel column chromatography (EtOAc/hexanes 1:1) to afford 0.1 g (54.3%) of **4a** as a white solid, m.p. 198–199°C. ¹H NMR (500 MHz, CDCl₃): δ 4.01 (t, 2 H, *J* = 6.0 Hz, CH₂-NCSe), 4.58 (t, 2 H, *J* = 6.0 Hz, CH₂N), 7.80 (t, 2 H, *J* = 8.5 Hz, Ar-*H*₅,*H*₈), 8.25 (dd, 2 H, *J* = 8.5, 1 Hz, Ar-*H*₆,*H*₇), 8.65 (dd, 2 H, *J* = 8.5 Hz, Ar-*H*₄,*H*₉); ¹³C NMR (125 MHz, CDCl₃) δ 164.06 (C=O), 164.02 (C=O), 134.5, 131.7, 131.7, 128.3, 127.1, 122.1 (aryl), 43.2 (CH₂-NCSe), 38.6 (NCH₂).

4.1.2.6. 3-Nitro[2-(2-isoselenocyanato-ethyl)]-benzo[de]isoquinoline-1,3-dione (4b).

Triphosgene (0.07 g, 0.23 mmol) in CH₂Cl₂ (5 mL) was added dropwise over a period of 1 h to a mixture of **3b** (0.15 g, 0.47 mmol), triethylamine (0.19 g, 1.87 mmol), and 4 Å molecular sieves in CH₂Cl₂ (10 mL). Resulting mixture was refluxed for 2 h and selenium powder (0.07 g, 0.93 mmol) was added at once. The refluxing was continued for another 30 h. The mixture was cooled and filtered, and the solvent was evaporated to yield the crude mixture was purified by column chromatography silica gel column chromatography (CH₂Cl₂/hexanes 1:1) to afford 0.1 g (56.1%)

of **4b** as a white solid, m.p. 195–196°C. ¹H NMR (500 MHz, CDCl₃): δ 4.16 (t, 2 H, *J* = 6.0 Hz, CH₂-NCSe), 4.42 (t, 2 H, *J* = 6.0 Hz, CH₂N), 8.09 (t, 1 H, *J* = 8 Hz, Ar-*H*₈), 8.73 (d, 1 H, *J* = 7.5 Hz, Ar-*H*₇), 8.81 (d, 1 H, *J* = 8.5 Hz, Ar-*H*₉), 8.98 (d, 1 H, *J* = 2.0 Hz, Ar-*H*₄), 9.51 (d, 1 H, *J* = 2 Hz, Ar-*H*₆); ¹³C NMR (125 MHz, CDCl₃) δ 163.0 (C=O), 162.4 (C=O), 146.5, 136.1, 135.0, 131.1, 130.3, 129.4, 129.2, 124.8, 124.1, 122.7 (aryl), 43.2 (CH₂-NCSe), 39.0 (NCH₂).

4.1.2.7. 2-(2-Isoselenocyanato-butyl)-benzo[de]isoquinoline-1,3-dione (**4c**).

Triphosgene (0.42 g, 1.41 mmol) in CH₂Cl₂ (10 mL) was added dropwise to a mixture containing **3c** (0.8 g, 2.69 mmol), triethylamine (1.14 g, 11.26 mmol) in CH₂Cl₂ (30 mL), and 4 Å molecular sieves for a period of 1 h. The resulting mixture was refluxed for 2 h and selenium powder (0.45 g, 5.6 mmol) was added at once and reflux continued for another 30 h. Crude product was purified by column chromatography silica gel column chromatography (EtOAc/hexanes 2:3) to afford 0.5 g (52.0 %) of **4c** as white solid, m.p. 159-160 °C. NMR (500 MHz, CDCl₃): δ 1.97-1.84 (m, 4 H, CH₂CH₂), 3.52 (t, 2 H, *J* = 5.5 Hz, CH₂-NCSe), 4.27 (t, 2 H, *J* = 6.0 Hz, CH₂N), 7.78 (t, 2 H, *J* = 6.5 Hz, Ar-*H*₅,*H*₈), 8.50 (d, 2 H, *J* = 7.0 Hz, Ar-*H*₆,*H*₇), 8.63 (d, 2 H, *J* = 6.0 Hz, Ar-*H*₄,*H*₉); ¹³C NMR (125 MHz, CDCl₃) δ 164.2 (2 × C=O), 134.1, 131.6, 131.4, 128.2, 127.0, 122.5 (aryl), 45.1 (CH₂-NCSe), 39.1 (NCH₂), 27.0 (CH₂), 25.2 (CH₂); HRMS (EI) *m/z* calcd for C₁₇H₁₄N₂O₂Se, 358.0215; found: 358.02048.

4.1.2.8. 2-(2-Isoselenocyanato-hexyl)-benzo[de]isoquinoline-1,3-dione (**4d**).

Triphosgene (0.22 g, 0.74 mmol) in CH₂Cl₂ (10 mL) was added dropwise to a mixture containing **3d** (0.5 g, 1.54 mmol), triethylamine (0.62 g, 6.2 mmol) in CH₂Cl₂ (15 mL), and 4 Å molecular

sieves for a period of 1 h. Resulting mixture was refluxed for 2 h and added selenium powder (0.25 g, 3.1 mmol) at once and continued to reflux for another 30 h. Crude product was purified by column chromatography silica gel column chromatography (CH₂Cl₂/hexanes 1:1) to afford 0.35 g (59.0%) of **4d** as white solid, m.p. 75–76 °C. NMR (500 MHz, CDCl₃): δ 1.48–1.59 (m, 4 H, CH₂CH₂), 1.74–1.81 (m, 4 H, CH₂CH₂) 3.41(t, 2 H, *J* = 3.5 Hz, CH₂-NCSe), 4.22 (t, 2 H, *J* = 7.5 Hz, CH₂N), 7.79 (t, 2 H, *J* = 8.0 Hz, Ar-*H*₅,*H*₈), 8.24 (d, 2 H, *J* = 8.0 Hz, Ar-*H*₆,*H*₇), 8.63(d, 2 H, 7.5 Hz, Ar-*H*₄,*H*₉); ¹³C NMR (125 MHz, CDCl₃) δ 164.2 (2 × C=O), 133.9, 131.6, 131.2, 128.2, 126.9, 122.7 (aryl), 40.1 (CH₂-NCSe), 29.3 (NCH₂), 29.0 (CH₂), 27.8 (CH₂), 26.2 (CH₂), 26.0 (CH₂).

4.1.2.9. 2-(2-Isoselenourea-ethyl)-benzo[de]isoquinoline-1,3-dione (**7a**).

A mixture of selenourea (0.21 g, 1.7 mmol) and **6a** (0.5 g, 1.7 mmol) in acetonitrile (30 mL) were refluxed for 4 h. The mixture was cooled to room temperature and the precipitate was filtered and washed with hot ethylacetate to get the title compound **7a** as a pale yellow solid, m.p. 290–291 °C. ¹H NMR (500 MHz, DMSO-*d*₆): δ 3.54 (t, 2 H, *J* = 7.0 Hz, CH₂-Se), 4.43 (t, 2 H, *J* = 7.0 Hz, CH₂N), 7.91 (t, 2 H, *J* = 8.0 Hz, Ar-*H*₅,*H*₈), 8.53 (dd, 4 H, *J* = 8.5, 7.5 Hz, Ar-*H*₆,*H*₇ & *H*₄,*H*₉), 9.14 (br s, 3 H, NH); ¹³C NMR (125 MHz, DMSO-*d*₆) δ 167.4 (C=O), 164.0 (C=O), 135.1, 131.8, 131.5, 127.9, 127.8, 122.3 (aryl), 39.4 (NCH₂), 25.2 (CH₂-Se); HRMS (EI) *m/z* calcd for C₁₅H₁₃N₃O₂Se, 347.0173; found: 347.0152.

4.1.2.10. 3-Nitro [2-(2-isoselenourea-ethyl)]-benzo[de]isoquinoline-1,3-dione (**7b**).

This compound was prepared from **6b** following the above method as a yellow solid, m.p. 209–210 °C. ¹H NMR (500 MHz, DMSO-*d*₆): δ 3.72 (t, 2 H, *J* = 7.0 Hz, CH₂-Se), 4.47 (t, 2 H, *J* = 7.0 Hz, CH₂N), 8.08 (t, 1 H, *J* = 8.0 Hz, Ar-*H*₈), 8.70 (d, 1 H, *J* = 8.0 Hz, Ar-*H*₇), 8.80 (d, 1 H, *J* =

8.0 Hz, Ar- H_9), 8.97 (d, 1 H, $J = 2.0$ Hz, Ar- H_4), 9.12 (br s, 3H, NH), 9.51 (d, 1 H, $J = 2$ Hz, Ar- H_6); ^{13}C NMR (125 MHz, DMSO- d_6) δ 163.1 (C=O), 162.6 (C=O), 146.3, 137.0, 134.6, 131.3, 130.4, 129.9, 129.8, 124.2, 123.5, 122.8 (aryl), 41.5 (NCH $_2$), 29.1 (CH $_2$ -Se); HRMS (EI) m/z calcd for C $_{15}$ H $_{12}$ N $_4$ O $_4$ Se, 391.0024; found: 391.0040.

4.2. Biological evaluation

4.2.1. Reagents and antibodies for biological evaluation

Antibodies for Western blot and immunohistochemistry purpose were ordered from following sources: Cell signaling technology (p-AKT (9271s), pan-Akt (4691s), pERK1/2 (4377s), ERK1/2 (9102s), caspase 3 (9668s), and p-H2A.X (2577s)); Sigma-Aldrich (β -actin (A5316)); ThermoFisher Scientific (Phalloidin/F-actin (A22284)) and Jackson Immuno Research (Alexa fluor 488 (711-545-152) and Donkey serum (017-000-002)). Thiazolyl Blue Tetrazolium Bromide (MTT) (M5655–500MG), Triton X-100 (93443), RNase A (R6513), and propidium iodide (PI) (P4170) were purchased from Sigma-Aldrich. DAPI mounting medium (17985-50) was purchased from Electron Microscopy Sciences.

4.2.2. Cell culture conditions

A375M, UACC903, CHL-1 and 1205Lu cell lines were maintained in DMEM medium supplemented with 10% fetal bovine serum (FBS) and 100 units/ml of penicillin and streptomycin at 37 °C and 5% CO $_2$. nHDFs were grown in Fibroblast Basal Medium (ATCC PCS-201-030) supplemented with Fibroblast Growth Kit–Serum-Free (ATCC PCS-201-040) and Penicillin-Streptomycin-Amphotericin B Solution (ATCC PCS-999-002). All the cell lines were obtained from ATCC.

4.2.3. Cell viability assay

MTT assay was used to measure the effect of the test compounds on cancer cell viability as described before [57]. In short, 3000 cells were plated in a 96 well plates and allowed to settle overnight in a 37 °C incubator. Next day, cells were treated with different concentrations of the test compounds in triplicates for different time points (24, 48 and 72 h) at 37 °C. MTT solution (20 µL of 5.0 mg/mL solution) was added to each well three hours prior to termination and incubated at 37 °C. The resultant formazan crystals at termination, were dissolved in DMSO, and the optical densities were measured at 570 nm and 630 nm using a 96-well multiscanner (Dynex Technologies, MRX Revelation; Chantilly, VA, USA). Non-linear regression analysis was performed using GraphPad Prism software to obtain the appropriate IC₅₀ values.

4.2.4. Docking method

The X-ray co-ordinates of Akt1 (pdb id: 3OCB) and human Topo-II α (pdb id: 3QX3) were downloaded from the protein data bank (www.rcsb.org), and refined using Prepare Protein module embedded in the Discovery Studio *ver* 4.0 [58]. This integrated module delete alternate conformations, add missing atoms and loops and protonates amino acid residues according to their predicted pK_a values. The co-crystallized ligands and water molecules of proteins were not considered in docking and removed using the DS. The minimization of proteins was performed by keeping the positions of hydrogen atoms constrained using the shake algorithm [59]. The conformational profile of compounds (NISC-6, ISC-4, and mitonafide) was explored using the Search Conformations algorithm (DS), and the lowest energy conformation was identified based on the CHARMM energy. Before docking, a binding sphere covering the binding site residues was generated for each protein. For Akt1, a sphere of diameter 15.0 Å with co-ordinates 12.5

(X), 2.4 (Y) and -17.2 (Z), and for topo-II, a sphere of diameter 10.1 Å with co-ordinates 32.8 (X), 95.9 (Y) and 51.7 (Z), were generated. The automated CDocker docking program [43] in DS was used to dock all compounds in the binding site of proteins using the default parameters. The conformational space of ligands was explored by the high temperature molecular dynamics method followed by their refinement using grid-based simulated annealing. Of the total poses identified, the best pose was selected based on scoring function (-CDocker energy), and subjected to the binding energy calculations.

4.2.5. Topo-II α inhibition studies in vitro

Topo-II α drug screening kit was used to test the ability of NISC-6 to directly inhibit TopoII α activity (Topogen, SKU TG1009-1). These was achieved by following the manufacturers instruction provided in the kit. In brief, supercoiled DNA provided in the kit was incubated with 4 units of human DNA Topo-II α (Topogen, SKU TG2000H-1) in assay buffer for 30 min at 37 °C. The reaction was terminated by addition of 10% sodium dodecyl sulfate. Further, digestion of the enzymes was performed by addition of proteinase K, followed by an incubation of 15 min at 37 °C. The mixture was ran on a 1% agrose gel for 1-2h. Following separation, the gel was stained with ethidium bromide for 2h and distained for 15 min in TAE buffer. Images of the gel were taken in presence of a UV lamp.

4.2.6. Western blot analysis

Melanoma cells (UACC903) treated with NISC-6 were subjected to whole cell lysis using RIPA lysis buffer (Thermo Scientific, USA) containing protease (Roche, USA) and phosphatase inhibitor cocktails (Sigma-Aldrich, USA) as described before [57]. Next, the whole cell lysates were centrifuged at 15,000 rpm for a duration of 10 minutes to remove any insoluble debris.

Resultant supernatant was stored -80 °C until use. NuPAGE ready-made gel 4-12% (Life Technologies, Carlsbad, CA) was used to resolve the lysates. After electrophoresis/SDS page, the resolved proteins were electro-transferred to PVDF membrane and blotted with the different antibodies. Enhanced Chemiluminescent (ECL) reagent (Life technologies, USA) was used to spot the protein of interest.

4.2.7. Immunocytochemistry for p-H2A.X.

Immunocytochemistry was performed to see the DNA damage at early time points in UACC903 cells treated with NISC-6. In brief, UACC903 cells (1.6×10^5) were seeded on top of a small cover slip in a 12 well cell culture plate in DMEM medium. Cells were incubated at 37 °C incubator with 5% CO₂ overnight for proper attachment to the coverslip. Following day, NISC-6 cells were treated with 5 μM NISC-6 or DMSO for 6 h. After 6 h, cells were fixed using 4% Formaldehyde Solution made in PBS for 15 min, followed by 1 x PBS wash. Cells were then blocked for 1 h using blocking medium (0.3% Triton X-100, 5% donkey serum, made in 1 x PBS) at room temperature in dark. Next coverslips were placed in primary anti-body (p-H2A.X diluted 1:500 in 1% BSA solution containing 0.3% Triton X-100) over night at 4 °C. Following day, primary antibody was washed with 1 x PBS wash. Subsequently, 0.03% H₂O₂ was added on top of the coverslip for 15 minutes at room temperature in dark. H₂O₂ was removed and replaced with secondary antibody solution (Alexa Fluor 488 at a dilution 1:500 in 1% BSA containing 0.3% triton X-100, and 1 unit of Phalloidin) and further incubated for 1 h. Secondary antibody was washed with 1x PBS and mounted on to glass slides with DAPI containing mounting medium. Slides were allowed to dry for 48 h and pictures were taken using the DELTA VISION microscope at 60X. Imaris 8.2 software was used for image processing.

4.2.8. Annexin V assay

To evaluate the effect of NISC-6 on apoptosis, UACC903 (1.6×10^5) cells were treated with increasing dose of NISC-6 or DMSO for 24 h. Stages of apoptosis, in adherent and floating cells, were quantified using the Muse Annexin V & Dead Cell kit with Muse cell analyzer (EMD Millipore, Billerica, MA, USA), according to manufacturer's protocol. The kit uses Annexin V stain to identify PS on the outer surface of the cells. The assay also contains a dead cell marker, 7-amino-actinomycin D (7-ADD), which is unable to enter cells with intact cell membrane (Millipore, Catalog No, MCH100105). Muse 1.4 software was used to analyze the data obtained from the equipment.

4.2.9. Caspase 3/7 activity assay

Activation of caspase 3/7 in melanoma cells upon exposure with NISC-6, was detected using Muse Caspase-3/7 Assay kit with Muse cell analyzer (EMD Millipore, Billerica, MA. USA) according to manufacturer's protocol. In brief, the assay contains a reagent namely NucView for recognition of activated caspase 3/7. This reagent is cell membrane permeable and hence can enter cells with intact plasma membrane. This reagent contains a DNA binding dye which is linked to a DEVD peptide substrate. DEVD inhibits the dye from binding to the DNA. DEVD in presence of active caspase 3/7 gets cleaved and hence DNA binding dye is released, which gives high fluorescence when excited (Ref Millipore, Catalog No. MCH100108). Further, the kit also contains a dead cell marker, 7-ADD, for detection of dead cells with compromised cell membrane. Data from Muse cell analyzer were analyzed using Muse 1.4 software.

4.2.10. Tumor inhibition studies *in vivo*

Animal experimentation was performed according to protocols approved by the Institutional Animal Care and Use Committee at The Pennsylvania State University College of Medicine. Tumor kinetics were measured by subcutaneous injection of 5×10^6 UACC 903 melanoma cells in 0.2 mL of DMEM supplemented with 10% FBS above both left and right flanks of 4-6 week old female athymic nude mice (Harlan Sprague Dawley, Indianapolis, IN). Six days after subcutaneous injection of UACC 903 cells, mice were randomly divided into control (DMSO) and experimental (NISC-6) groups (5 mice/group; 2 tumors/mouse). Mice were treated i.p. with DMSO or NISC-6 (0.6 μ mole) three times per week. The dimensions of the developing tumors (using calipers) and body weight were measured three times a week and the size estimated in cubic millimeters.

Acknowledgment

The authors thank the Department of Pharmacology, Penn State College of Medicine, and Penn State Hershey Cancer Institute for financial support. The authors thank Solution Phase NMR Facility (Dr. Jyh-Ming Lin) at Core Research Facilities of the Pennsylvania State University, College of Medicine. The authors acknowledge the Centre for High Performance Computing for computer software and supercomputer facility, an initiative supported by the Department of Science and Technology of South Africa.

Supplementary Material. Copies of the ^1H NMR and ^{13}C NMR spectra for new compounds **4a**, **4b**, **4c**, **4d**, **7a** and **7b**. Figure S1 showing (a) overlay of the poses of co-crystallized ligand (etoposide) present docking simulation for Akt1, (b) overlay of the poses of co-crystallized ligand (EVP1) and present docking simulation for topo-II.

References:

- [1] D.M. Parkin, D. Mesher, P. Sasieni, 13. Cancers attributable to solar (ultraviolet) radiation exposure in the UK in 2010, *Br. J. Cancer* 105 Suppl 2 (2011) S66-69.
- [2] A. Jemal, R. Siegel, J. Xu, E. Ward, Cancer statistics, 2010, *CA Cancer J. Clin.* 60 (2010) 277-300.
- [3] Cancer Facts and Figures 2017. American Cancer Society.
- [4] M.S. Soengas, S.W. Lowe, Apoptosis and melanoma chemoresistance, *Oncogene* 22 (2003) 3138-3151.
- [5] J.T. Lee, L. Li, P.A. Brafford, M. Eijnden, M.B. Halloran, K. Sproesser, N.K. Haass, K.S. Smalley, J. Tsai, G. Bollag, M. Herlyn, PLX4032, a potent inhibitor of the B-Raf V600E oncogene, selectively inhibits V600E-positive melanomas, *Pigment Cell Melanoma Res.* 23 (2010) 820-827.
- [6] J. Tsai, J.T. Lee, W. Wang, J. Zhang, H. Cho, S. Mamo, R. Bremer, S. Gillette, J. Kong, N.K. Haass, K. Sproesser, L. Li, K.S. Smalley, D. Fong, Y.L. Zhu, A. Marimuthu, H. Nguyen, B. Lam, J. Liu, I. Cheung, J. Rice, Y. Suzuki, C. Luu, C. Settachatgul, R. Shellooe, J. Cantwell, S.H. Kim, J. Schlessinger, K.Y. Zhang, B.L. West, B. Powell, G. Habets, C. Zhang, P.N. Ibrahim, P. Hirth, D.R. Artis, M. Herlyn, G. Bollag, Discovery of a selective inhibitor of oncogenic B-Raf kinase with potent antimelanoma activity, *Proc. Natl. Acad. Sci. U. S. A.* 105 (2008) 3041-3046.
- [7] G. Bollag, P. Hirth, J. Tsai, J. Zhang, P.N. Ibrahim, H. Cho, W. Spevak, C. Zhang, Y. Zhang, G. Habets, E.A. Burton, B. Wong, G. Tsang, B.L. West, B. Powell, R. Shellooe, A. Marimuthu, H. Nguyen, K.Y. Zhang, D.R. Artis, J. Schlessinger, F. Su, B. Higgins, R. Iyer, K. D'Andrea, A. Koehler, M. Stumm, P.S. Lin, R.J. Lee, J. Grippo, I. Puzanov, K.B. Kim, A. Ribas, G.A. McArthur, J.A. Sosman, P.B. Chapman, K.T. Flaherty, X. Xu, K.L. Nathanson, K. Nolop, Clinical efficacy of a RAF inhibitor needs broad target blockade in BRAF-mutant melanoma, *Nature* 467 (2010) 596-599.
- [8] P.B. Chapman, A. Hauschild, C. Robert, J.B. Haanen, P. Ascierto, J. Larkin, R. Dummer, C. Garbe, A. Testori, M. Maio, D. Hogg, P. Lorigan, C. Lebbe, T. Jouary, D. Schadendorf, A. Ribas, S.J. O'Day, J.A. Sosman, J.M. Kirkwood, A.M. Eggermont, B. Dreno, K. Nolop, J. Li, B. Nelson, J. Hou, R.J. Lee, K.T. Flaherty, G.A. McArthur, Improved survival with vemurafenib in melanoma with BRAF V600E mutation, *N. Engl. J. Med.* 364 (2011) 2507-2516.
- [9] K.T. Flaherty, I. Puzanov, K.B. Kim, A. Ribas, G.A. McArthur, J.A. Sosman, P.J. O'Dwyer, R.J. Lee, J.F. Grippo, K. Nolop, P.B. Chapman, Inhibition of mutated, activated BRAF in metastatic melanoma, *N. Engl. J. Med.* 363 (2010) 809-819.

- [10] R. Nazarian, H. Shi, Q. Wang, X. Kong, R.C. Koya, H. Lee, Z. Chen, M.K. Lee, N. Attar, H. Sazegar, T. Chodon, S.F. Nelson, G. McArthur, J.A. Sosman, A. Ribas, R.S. Lo, Melanomas acquire resistance to B-RAF(V600E) inhibition by RTK or N-RAS upregulation, *Nature* 468 (2010) 973-977.
- [11] P. Hersey, K.S. Smalley, A. Weeraratna, M. Bosenberg, X.D. Zhang, N.K. Haass, E. Paton, G. Mann, R.A. Scolyer, T. Tuting, Meeting report from the 7th International Melanoma Congress, Sydney, November, 2010, *Pigment Cell Melanoma Res.* 24 (2011) e1-15.
- [12] L. Min, F.S. Hodi, Anti-PD1 following ipilimumab for mucosal melanoma: durable tumor response associated with severe hypothyroidism and rhabdomyolysis, *Cancer Immunol. Res.* 2 (2014) 15-18.
- [13] A.K. Sharma, A. Sharma, D. Desai, S.V. Madhunapantula, S.J. Huh, G.P. Robertson, S. Amin, Synthesis and anticancer activity comparison of phenylalkyl isoselenocyanates with corresponding naturally occurring and synthetic isothiocyanates, *J. Med. Chem.* 51 (2008) 7820-7826.
- [14] A. Sharma, A.K. Sharma, S.V. Madhunapantula, D. Desai, S.J. Huh, P. Mosca, S. Amin, G.P. Robertson, Targeting Akt3 signaling in malignant melanoma using isoselenocyanates, *Clin. Cancer Res.* 15 (2009) 1674-1685.
- [15] U.H. Sk, A.S. Gowda, M.A. Crampsie, J.K. Yun, T.E. Spratt, S. Amin, A.K. Sharma, Development of novel naphthalimide derivatives and their evaluation as potential melanoma therapeutics, *Eur. J. Med. Chem.* 46 (2011) 3331-3338.
- [16] N. Nguyen, A. Sharma, A.K. Sharma, D. Desai, S.J. Huh, S. Amin, C. Meyers, G.P. Robertson, Melanoma chemoprevention in skin reconstructs and mouse xenografts using isoselenocyanate-4, *Cancer Prev. Res.* 4 (2011) 248-258.
- [17] P.M. Cinciripini, S.S. Hecht, J.E. Henningfield, M.W. Manley, B.S. Kramer, Tobacco addiction: implications for treatment and cancer prevention, *J. Natl. Cancer Inst.* 89 (1997) 1852-1867.
- [18] A. Drewnowski, C. Gomez-Carneros, Bitter taste, phytonutrients, and the consumer: a review, *Am. J. Clin. Nutr.* 72 (2000) 1424-1435.
- [19] J.W. Fahey, A.T. Zalcman, P. Talalay, The chemical diversity and distribution of glucosinolates and isothiocyanates among plants, *Phytochemistry* 56 (2001) 5-51.
- [20] C.W. Beecher, Cancer preventive properties of varieties of Brassica oleracea: a review, *Am J. Clin. Nutr.* 59 (1994) 1166S-1170S.

- [21] P. Talalay, J.W. Fahey, Phytochemicals from cruciferous plants protect against cancer by modulating carcinogen metabolism, *J. Nutr.* 131 (2001) 3027S-3033S.
- [22] A.K. Sharma, C.L. Kline, A. Berg, S. Amin, R.B. Irby, The Akt inhibitor ISC-4 activates prostate apoptosis response protein-4 and reduces colon tumor growth in a nude mouse model, *Clin. Cancer Res.* 17 (2011) 4474-4483.
- [23] M.A. Crampsie, N. Jones, A. Das, C. Aliaga, D. Desai, P. Lazarus, S. Amin, A.K. Sharma, Phenylbutyl isoselenocyanate modulates phase I and II enzymes and inhibits 4-(methylnitrosamino)-1-(3-pyridyl)-1-butanone-induced DNA adducts in mice, *Cancer Prev. Res.* 4 (2011) 1884-1894.
- [24] M.F. Brana, A. Ramos, Naphthalimides as anti-cancer agents: synthesis and biological activity, *Curr. Med. Chem. Anticancer Agents* 1 (2001) 237-255.
- [25] E. Van-Quaquebeke, T. Mahieu, P. Dumont, J. Dewelle, F. Ribaucour, G. Simon, S. Sauvage, J.F. Gaussin, J. Tuti, M. El Yazidi, F. Van Vynckt, T. Mijatovic, F. Lefranc, F. Darro, R. Kiss, 2,2,2-Trichloro-N-({2-[2-(dimethylamino)ethyl]-1,3-dioxo-2,3-dihydro-1H-benz[de]isoquinolin-5-yl}carbonyl)acetamide (UNBS3157), a novel nonhematotoxic naphthalimide derivative with potent antitumor activity, *J. Med. Chem.* 50 (2007) 4122-4134.
- [26] V.K. Malviya, P.Y. Liu, D.S. Alberts, E.A. Surwit, J.B. Craig, E.V. Hannigan, Evaluation of amonafide in cervical cancer, phase II. A SWOG study, *J. Clin. Oncol.* 15 (1992) 41-44.
- [27] I. Ott, X. Qian, Y. Xu, D.H. Vleck, I.J. Marques, D. Kubutat, J. Will, W.S. Sheldrick, P. Jesse, A. Prokop, C.P. Bagowski, A gold(I) phosphine complex containing a naphthalimide ligand functions as a TrxR inhibiting antiproliferative agent and angiogenesis inhibitor, *J. Med. Chem.* 52 (2009) 763-770.
- [28] R. Rosell, J. Carles, A. Abad, N. Ribelles, A. Barnadas, A. Benavides, M. Martin, Phase I study of mitonafide in 120 hour continuous infusion in non-small cell lung cancer, *Invest. New Drugs* 10 (1992) 171-175.
- [29] M.F. Brana, M. Cacho, M.A. Garcia, B. Pascual-Teresa, A. Ramos, N. Acero, F. Llinares, D. Munoz-Mingarro, C. Abradelo, M.F. Rey-Stolle, M. Yuste, Synthesis, antitumor activity, molecular modeling, and DNA binding properties of a new series of imidazonaphthalimides, *J. Med. Chem.* 45 (2002) 5813-5816.
- [30] M.F. Brana, J.M. Castellano, C.M. Roldan, A. Santos, D. Vazquez, A. Jimenez, Synthesis and mode(s) of action of a new series of imide derivatives of 3-nitro-1,8 naphthalic acid, *Cancer Chemother Pharmacol.* 4 (1980) 61-66.

- [31] E. Diaz-Rubio, M. Martin, J.M. Lopez-Vega, A. Casado, A. Benavides, Phase I study of mitonafide with a 3-day administration schedule: early interruption due to severe central nervous system toxicity, *Invest. New Drugs* 12 (1994) 277-281.
- [32] M. Llombart, A. Poveda, E. Forner, C. Fernandez-Martos, C. Gaspar, M. Munoz, T. Olmos, A. Ruiz, V. Soriano, A. Benavides, et al., Phase I study of mitonafide in solid tumors, *Invest. New Drugs* 10 (1992) 177-181.
- [33] R. Saez, J.B. Craig, J.G. Kuhn, G.R. Weiss, J. Koeller, J. Phillips, K. Havlin, G. Harman, J. Hardy, T.J. Melink, et al., Phase I clinical investigation of amonafide, *J. Clin. Oncol.* 7 (1989) 1351-1358.
- [34] S. O'Brien, J.A. Benvenuto, E. Estey, M. Beran, T.B. Felder, M. Keating, Phase I clinical investigation of benziisoquinolinedione (amonafide) in adults with refractory or relapsed acute leukemia, *Cancer Res.* 51 (1991) 935-938.
- [35] M.A. Crampsie, M.K. Pandey, D. Desai, J. Spallholz, S. Amin, A.K. Sharma, Phenylalkyl isoselenocyanates vs phenylalkyl isothiocyanates: thiol reactivity and its implications, *Chem. Biol. Interact.* 200 (2012) 28-37.
- [36] S.V. Madhunapantula, D. Desai, A. Sharma, S.J. Huh, S. Amin, G.P. Robertson, PBISe, a novel selenium-containing drug for the treatment of malignant melanoma, *Mol. Cancer Ther.* 7 (2008) 1297-1308.
- [37] V. Alcolea, D. Plano, D.N. Karelia, J.A. Palop, S. Amin, C. Sanmartin, A.K. Sharma, Novel seleno- and thio-urea derivatives with potent in vitro activities against several cancer cell lines, *Eur. J. Med. Chem.* 113 (2016) 134-144.
- [38] C.Y. Chung, S.V. Madhunapantula, D. Desai, S. Amin, G.P. Robertson, Melanoma prevention using topical PBISe, *Cancer Prev. Res.* 4 (2011) 935-948.
- [39] E.P. Garvey, J.A. Oplinger, G.J. Tanoury, P.A. Sherman, M. Fowler, S. Marshall, M.F. Harmon, J.E. Paith, E.S. Furfine, Potent and selective inhibition of human nitric oxide synthases. Inhibition by non-amino acid isothioureas, *J. Biol. Chem.* 269 (1994) 26669-26676.
- [40] V. Tumiatti, A. Milelli, A. Minarini, M. Micco, A. Gasperi Campani, L. Roncuzzi, D. Baiocchi, J. Marinello, G. Capranico, M. Zini, C. Stefanelli, C. Melchiorre, Design, synthesis, and biological evaluation of substituted naphthalene imides and diimides as anticancer agent, *J. Med. Chem.* 52 (2009) 7873-7877.
- [41] M.F. Brana, A.M. Sanz, J.M. Castellano, C.M. Roldan, C. Roldan, Synthesis and cytostatic activity of benz(de)-isoquinolines-1,3-diones: Structure activity relationships, *Eur. J. Med. Chem.* 16 (1981) 207-212.

- [42] J.G. Fernández-Bolaños, López, O., Ulgar, V., Maya, I., and Fuentes, J. , Synthesis of *O*-unprotected glycosyl selenoureas. A new access to bicyclic sugar isoureas. , *Tetrahedron Lett.* 45 (2004) 4081-4084.
- [43] G. Wu, D.H. Robertson, C.L. Brooks, 3rd, M. Vieth, Detailed analysis of grid-based molecular docking: A case study of CDOCKER-A CHARMM-based MD docking algorithm, *J. Comput. Chem.* 24 (2003) 1549-1562.
- [44] E.P. Rogakou, D.R. Pilch, A.H. Orr, V.S. Ivanova, W.M. Bonner, DNA double-stranded breaks induce histone H2AX phosphorylation on serine 139, *J. Biol. Chem.* 273 (1998) 5858-5868.
- [45] A. Kurose, T. Tanaka, X. Huang, H.D. Halicka, F. Traganos, W. Dai, Z. Darzynkiewicz, Assessment of ATM phosphorylation on Ser-1981 induced by DNA topoisomerase I and II inhibitors in relation to Ser-139-histone H2AX phosphorylation, cell cycle phase, and apoptosis, *Cytometry A.* 68 (2005) 1-9.
- [46] X. Huang, M. Okafuji, F. Traganos, E. Luther, E. Holden, Z. Darzynkiewicz, Assessment of histone H2AX phosphorylation induced by DNA topoisomerase I and II inhibitors topotecan and mitoxantrone and by the DNA cross-linking agent cisplatin, *Cytometry A.* 58 (2004) 99-110.
- [47] H. Helmbach, E. Rossmann, M.A. Kern, D. Schadendorf, Drug-resistance in human melanoma, *Int. J. Cancer* 93 (2001) 617-622.
- [48] G.P. Robertson, Functional and therapeutic significance of Akt deregulation in malignant melanoma, *Cancer Metast. Rev.* 24 (2005) 273-285.
- [49] R.C. Taylor, S.P. Cullen, S.J. Martin, Apoptosis: controlled demolition at the cellular level, *Nat. Rev. Mol. Cell Biol.*, 9 (2008) 231-241.
- [50] D.F. Veber, S.R. Johnson, H.Y. Cheng, B.R. Smith, K.W. Ward, K.D. Kopple, Molecular properties that influence the oral bioavailability of drug candidates, *J. Med. Chem.* 45 (2002) 2615-2623.
- [51] C.A. Lipinski, F. Lombardo, B.W. Dominy, P.J. Feeney, Experimental and computational approaches to estimate solubility and permeability in drug discovery and development settings, *Adv. Drug Deliv. Rev.* 46 (2001) 3-26.
- [52] P. Ertl, B. Rohde, P. Selzer, Fast calculation of molecular polar surface area as a sum of fragment-based contributions and its application to the prediction of drug transport properties, *J. Med. Chem.* 43 (2000) 3714-3717.

- [53] K. Palm, P. Stenberg, K. Luthman, P. Artursson, Polar molecular surface properties predict the intestinal absorption of drugs in humans, *Pharm. Res.* 14 (1997) 568-571.
- [54] M. Licchelli, A.O. Biroli, A. Poggi, D. Sacchi, C. Sangermani, M. Zema, Excimer emission induced by metal ion coordination in 1,8-naphthalimide-tethered iminopyridine ligands, *J. Chem. Soc., Dalton Trans.* 23 (2003) 4537-4545.
- [55] S.U. Hossain, S. Sengupta, S. Bhattacharya, Synthesis and evaluation of antioxidative properties of a series of organoselenium compounds, *Bioorg. Med. Chem.* 13 (2005) 5750-5758.
- [56] M.C. Elliott, E. Williams, Synthesis and reactions of partially reduced bisoquinolines, *Org. Biomol. Chem.*, 1 (2003) 3038-3047.
- [57] D. Plano, D.N. Karelia, M.K. Pandey, J.E. Spallholz, S. Amin, A.K. Sharma, Design, Synthesis, and Biological Evaluation of Novel Selenium (Se-NSAID) Molecules as Anticancer Agents, *J. Med. Chem.* 59 (2016) 1946-1959.
- [58] A. Casado, R. Rosell, R. Garcia-Gomez, E. Diaz-Rubio, G. Perez-Manga, A. Font, A. Benavides, M. Martin, Phase II study of mitonafide in non-small cell lung cancer (NSCLC), *Invest. New Drugs* 14 (1996) 415-417.
- [59] J.P. Rychaert, G. Ciccotti, H.J.C. Berendsen, Numerical integration of the Cartesian equations of motion of a system with constraints: Molecular dynamics of n-alkanes, *J. Comput. Phys.* 23 (1977) 327-341.

Highlights

- Novel naphthalamide-isoselnocyanate and -selenourea analogs were synthesized
- The isoselnocyanate analog NISC-6 was identified as the most effective compound
- NISC-6 inhibited growth of melanoma cell lines with both WT or mutant BRAF
- NISC-6 was dual inhibitor of in vitro Topo-II α activity and Akt pathway
- NISC-6 induced apoptotic cell death in melanoma cells
- NISC-6 effectively inhibited tumor growth in a melanoma xenograft mouse model